Chapter 8

FREQUENCY DOMAIN PROPERTIES OF LINEAR INTERVAL SYSTEMS

In this chapter we develop some useful frequency domain properties of systems containing uncertain parameters. The Generalized Kharitonov Theorem of the last chapter introduced a set of one parameter extremal plants which completely characterize the frequency domain behaviour of linear interval systems. We show here that this extremal set can be used to exactly calculate the uncertainty template at each frequency as well as the Bode, Nyquist and Nichols envelopes of the system. We also prove that the worst case gain, phase, and parametric stability margins of control systems containing such a plant occur over this extremal set. The utility of these tools in robust classical control design is illustrated by examples.

8.1 INTRODUCTION

Frequency response methods play a fundamental role in the fields of control, communications and signal processing. Classical control focuses on the frequency domain properties of control systems and has developed design methods based on simple but powerful graphical tools such as the Nyquist plot, Bode plots, and Nichols Chart. These techniques are well known and are popular with practicing engineers. However, they were developed for a fixed nominal system and in general are inapplicable when several uncertain parameters are present. In these situations it is necessary to evaluate the frequency domain behaviour of the *entire family* of systems in order to effectively carry out analysis and design.

A brute force approach to this problem (grid the uncertainty set) can be avoided by assuming a certain amount of structure for the perturbations even if such an assumption introduces some conservatism. In this chapter we shall consider the class of linear interval systems where the uncertain parameters lie in intervals and appear linearly in the numerator and denominator coefficients of the transfer functions. For

example, the family of transfer functions

$$\mathbf{G}(s) = \frac{4s^3 + \alpha_2 s^2 + \alpha_1 s + 5}{s^4 + 10\beta_3 s^3 + \beta_2 s^2 + (\beta_1 + 2\gamma_1)s}$$

where $\alpha_2, \alpha_1, \beta_3, \beta_2, \beta_1, \gamma_1$ vary in independent intervals is a linear interval system containing six interval parameters. In this example, the uncertainty template $\mathbf{G}(j\omega)$ at each frequency ω is a complex plane set generated by the parameter vector ranging over the six dimensional parameter box. With the results to be developed in this chapter we will be able to replace $\mathbf{G}(s)$ by a subset of systems $\mathbf{G}_{\mathrm{E}}(s)$. This extremal subset will allow us to constructively generate the *exact* boundary of the uncertainty template by means of a set of *one parameter* problems. These extremal systems will allow us to exactly calculate the boundaries of the Bode, Nyquist and Nichols plots of all transfer functions in the control system. They also can be used to calculate the worst case gain, phase, and parametric stability margins over the uncertain set of parameters. The utility of these concepts in control system design is illustrated by giving examples which robustify classical design techniques by incorporating parametric uncertainty.

We begin by considering an interval plant connected to a fixed feedback controller and develop the appropriate mathematical machinery for this system. The generalized Kharitonov segments introduced in Chapter 7 serve to define the extremal systems. Using these systems, we calculate the boundaries of the image sets of various system transfer functions evaluated at $s = j\omega$. These include the characteristic polynomial, open and closed loop transfer functions, sensitivity and complementary sensitivity and disturbance transfer functions. We also evaluate the worst case stability margins using these extremal systems. These results depend on some simple geometric facts regarding the sum and quotients of complex plane sets. We then generalize these results to the larger class of linear interval systems using essentially the same geometric ideas.

8.2 INTERVAL CONTROL SYSTEMS

Consider the feedback system shown in Figure 8.1 with

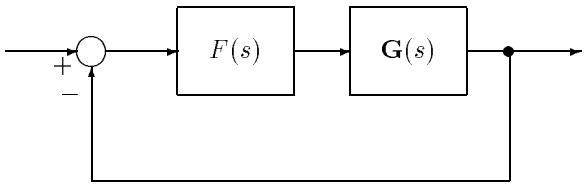

Figure 8.1. A unity feedback interval control system

$$F(s) := \frac{F_1(s)}{F_2(s)}, \qquad G(s) := \frac{N(s)}{D(s)}. \tag{8.1}$$

We suppose that $F(s)$ is fixed but $G(s)$ contains uncertain real parameters which appear as the coefficients of $N(s)$ and $D(s)$. Write

$$\begin{aligned} D(s) &:= a_0 + a_1 s + a_2 s^2 + a_3 s^3 + \cdots + a_{n-1} s^{n-1} + a_n s^n \\ N(s) &:= b_0 + b_1 s + b_2 s^2 + b_3 s^3 + \cdots + b_{m-1} s^{m-1} + b_m s^m \end{aligned} \tag{8.2}$$

where $a_k \in [a_k^-, \bar{a}_k^+]$, for $k \in \underline{n} := \{1, \cdots, n\}$ and $b_k \in [b_k^-, \bar{b}_k^+]$, for $k \in \underline{m}$. Let us define the interval polynomial sets

$$\begin{aligned} \mathbf{D}(s) &:= \{D(s) \ : \ a_0 + a_1 s + a_2 s^2 + \cdots + a_n s^n, \ a_k \in [a_k^-, a_k^+], \text{ for } \ k \in \underline{n}\} \\ \mathbf{N}(s) &:= \{N(s) \ : \ b_0 + b_1 s + b_2 s^2 + \cdots + b_m s^m, \ b_k \in [b_k^-, b_k^+], \text{ for } \ k \in \underline{m}\} \end{aligned}$$

and the corresponding set of *interval systems*:

$$\mathbf{G}(s) := \left\{ \ \frac{N(s)}{D(s)} \ : \ (N(s), D(s)) \in (\mathbf{N}(s) \mathrm{x} \mathbf{D}(s)) \ \right\}. \tag{8.3}$$

We refer to the unity feedback system in Figure 8.1 as an *interval control system*. For simplicity, we will use the notational convention

$$\mathbf{G}(s) = \frac{\mathbf{N}(s)}{\mathbf{D}(s)} \tag{8.4}$$

to denote the family (8.3). The characteristic polynomial of the system is

$$\delta(s) := F_1(s) N(s) + F_2(s) D(s) \tag{8.5}$$

and the set of system characteristic polynomials can be written as

$$\mathbf{\Delta}(s) := F_1(s) \mathbf{N}(s) + F_2(s) \mathbf{D}(s). \tag{8.6}$$

The control system is robustly stable if each polynomial in $\mathbf{\Delta}(s)$ is of the same degree and is Hurwitz. This is precisely the type of robust stability problem dealt with in the Generalized Kharitonov Theorem (GKT) of the last chapter, where we showed that Hurwitz stability of the control system over the set $\mathbf{G}(s)$ could be reduced to testing over the much smaller extremal set of systems $\mathbf{G}_{\mathrm{E}}(s)$.

Following the notation of the last chapter, let $\mathcal{K}_N(s)$ and $\mathcal{K}_D(s)$ denote Kharitonov polynomials associated with $\mathbf{N}(s)$ and $\mathbf{D}(s)$, and let $\mathcal{S}_N(s)$ and $\mathcal{S}_D(s)$ denote the corresponding sets of Kharitonov segments. Recall that these segments are pairwise convex combinations of Kharitonov polynomials sharing a common even or odd part. Define the *extremal subsets*, using the above notational convention:

$$\mathbf{G}_{\mathrm{E}}(s) := \frac{\mathcal{K}_N(s)}{\mathcal{S}_D(s)} \cup \frac{\mathcal{S}_N(s)}{\mathcal{K}_D(s)} \qquad \text{(extremal systems)} \tag{8.7}$$

$$\mathbf{G}_{\mathrm{K}}(s) := \frac{\mathcal{K}_N(s)}{\mathcal{K}_D(s)} \qquad \text{(Kharitonov systems)}. \tag{8.8}$$

We shall say that $F(s)$ satisfies the *vertex condition* if the polynomials $F_i(s)$ are of the form

$$F_i(s) := s^{t_i}(a_i s + b_i)U_i(s)R_i(s), \quad i = 1, 2 \tag{8.9}$$

where t_i are nonnegative integers, a_i, b_i are arbitrary real numbers, $U_i(s)$ is an anti-Hurwitz polynomial, and $R_i(s)$ is an even or odd polynomial. We recall the result given by GKT.

Theorem 8.1 *The control system of Figure 8.1 is robustly stable that is stable for all $G(s) \in \mathbf{G}(s)$ if and only if it is stable for all $G(s) \in \mathbf{G}_{\mathrm{E}}(s)$. If in addition $F(s)$ satisfies the vertex condition, robust stability holds if the system is stable for each $G(s) \in \mathbf{G}_{\mathrm{K}}(s)$.*

The GKT thus reduces the problem of verifying robust stability over the multiparameter set $\mathbf{G}(s)$ to a set of one parameter stability problems over $\mathbf{G}_E(s)$ in general, and under the special conditions on $F(s)$ stated, to the vertex set $\mathbf{G}_K(s)$. In the rest of this chapter we shall show that the systems $\mathbf{G}_{\mathrm{E}}(s)$ and $\mathbf{G}_{\mathrm{K}}(s)$ enjoy many other useful boundary and extremal properties. They can be constructively used to carry out frequency response calculations in control system analysis and design. In fact, it will turn out that most of the important system properties such as worst case stability and performance margins over the set of uncertain parameters can be determined by replacing $G(s) \in \mathbf{G}(s)$ by the elements of $G(s) \in \mathbf{G}_{\mathrm{E}}(s)$. In some special cases one may even replace $G(s)$ by the elements of $\mathbf{G}_{\mathrm{K}}(s)$. The results are first developed for interval plants for the sake of simplicity. They hold for the more general class of linear interval systems as indicated in section 8.6.

8.3 FREQUENCY DOMAIN PROPERTIES

In order to carry out frequency response analysis and design incorporating robustness with respect to parameter uncertainty we need to be able to determine the complex plane images of various parametrized sets. In this section we will develop some computationally efficient procedures to generate such sets. We shall first consider the complex plane images of $\mathbf{\Delta}(s)$ and $\mathbf{G}(s)$ at $s = j\omega$. These sets, called uncertainty templates, are denoted $\mathbf{\Delta}(j\omega)$ and $\mathbf{G}(j\omega)$. Since $\mathbf{N}(s)$ and $\mathbf{D}(s)$ are interval families, $\mathbf{N}(j\omega)$ and $\mathbf{D}(j\omega)$ are axis parallel rectangles in the complex plane. $F_1(j\omega)\mathbf{N}(j\omega)$ and $F_2(j\omega)\mathbf{D}(j\omega)$ are likewise rotated rectangles in the complex plane. Thus $\mathbf{\Delta}(j\omega)$ is the complex plane sum of two rectangles whereas $\mathbf{G}(j\omega)$ is the quotient of two rectangles. We assume here that $0 \notin \mathbf{D}(j\omega)$. If this assumption fails to hold we can always "indent" the $j\omega$ axis to exclude those values of ω which violate the assumption. Therefore, throughout this chapter we will make the standing assumption that the denominator of any quotients exclude zero.

The next lemma will show us how to evaluate the sum and quotient of two complex plane polygons Q_1 and Q_2 with vertex sets V_1 and V_2, and edge sets E_1 and E_2, respectively. Let $\partial(\cdot)$ denote the boundary of the complex plane set $(\cdot)$.

Lemma 8.1

$$(a) \qquad \partial(Q_1 + Q_2) \subset (V_1 + E_2) \cup (E_1 + V_2)$$
$$(b) \qquad \partial\left(\frac{Q_1}{Q_2}\right) \subset \frac{E_1}{V_2} \cup \frac{V_1}{E_2}.$$

Proof. (a) From simple complex plane geometry the complex sum of two straight lines is generated by adding vertex-segment pairs. Thus the result is true for this case. For the general case it is known that $\partial(Q_1 + Q_2) \subset \partial Q_1 + \partial Q_2$. Then without loss of generality we let ∂Q_1 be an edge and ∂Q_2 be another edge and use the previous argument. This proves part (a) of the lemma.

(b) First, we establish that $z \in \partial\left(\frac{Q_1}{Q_2}\right)$ if and only if $0 \in \partial\,(Q_1 - zQ_2)$. Indeed if $z_0 \in \partial\left(\frac{Q_1}{Q_2}\right)$, then for every $\epsilon > 0$ the open disc $|z - z_0| < \epsilon$ contains points z such that $z \notin \frac{Q_1}{Q_2}$. Thus, $0 \notin Q_1 - zQ_2$. However, $0 \in Q_1 - z_0Q_2$ since $z_0 \in \frac{Q_1}{Q_2}$. By continuity of $Q_1 - zQ_2$ with respect to z at z_0, it follows that $0 \in \partial(Q_1 - z_0Q_2)$. Now suppose conversely that $0 \in \partial(Q_1 - z_0Q_2)$. Then for every $\epsilon > 0$ the disc of radius ϵ centered at the origin contains points q such that $q \notin Q_1 - z_0Q_2$. By continuity of the mapping $\frac{Q_1}{Q_2} \longrightarrow Q_1 - zQ_2$ with respect to z the inverse image z of the point q is close to z_0. But this point $z \notin \frac{Q_1}{Q_2}$ since $0 \notin Q_1 - zQ_2$. However, z can be chosen to be arbitrarily close to z_0. Since $z_0 \in \frac{Q_1}{Q_2}$, it follows that $z_0 \in \partial\left(\frac{Q_1}{Q_2}\right)$.

Now,

$$z \in \partial\left(\frac{Q_1}{Q_2}\right) \Longleftrightarrow 0 \in \partial(Q_1 - zQ_2) \Longleftrightarrow 0 \in (V_1 - zE_2) \cup (E_1 - zV_2)$$
$$\Longleftrightarrow z \in \frac{V_1}{E_2} \cup \frac{E_1}{V_2}. \tag{8.10}$$

♣

This lemma shows us the interesting fact that the boundaries of sums and quotients of two polygons can be determined by sums and quotients of the corresponding vertex-edge pairs. Figure 8.2 illustrates that the boundaries of the sum of two four sided polygons are obtained by generating the sum of all segment-edge pairs. Similarly, Figure 8.3 shows the sum of two general polygons.

It can be shown that the inverse image of a line segment which excludes the origin, is an arc of a circle passing through the origin (Exercise 8.4). This is shown in Figure 8.4. Therefore the inverse image of a polygon is bounded by such arcs as shown in Figure 8.5.

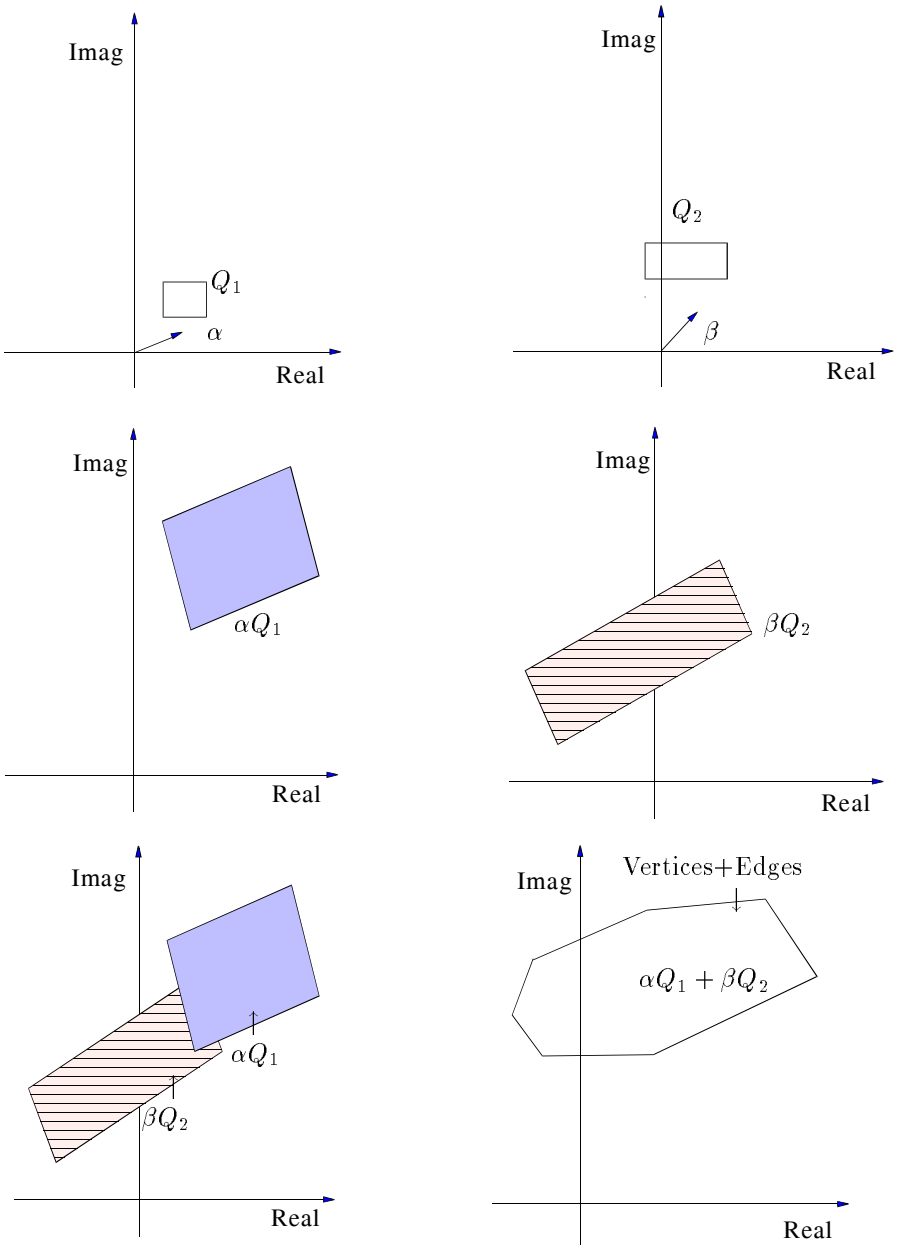

Figure 8.2. Illustration of sum of two polygons

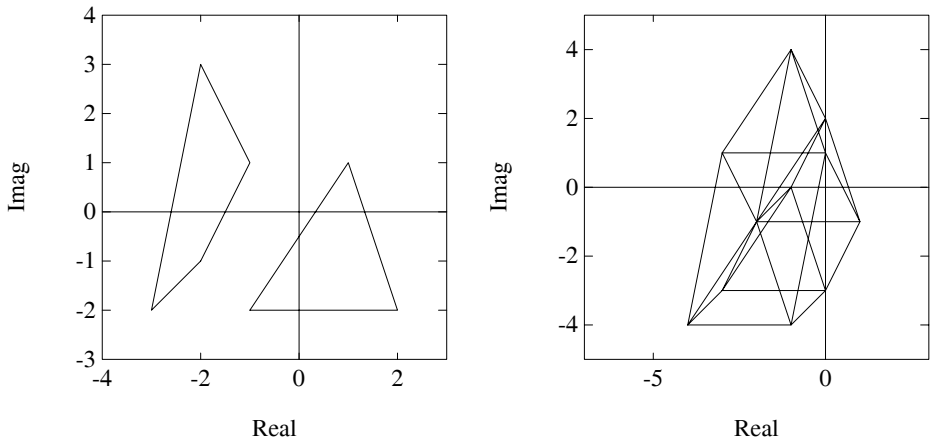

Figure 8.3. Sum of two polygons

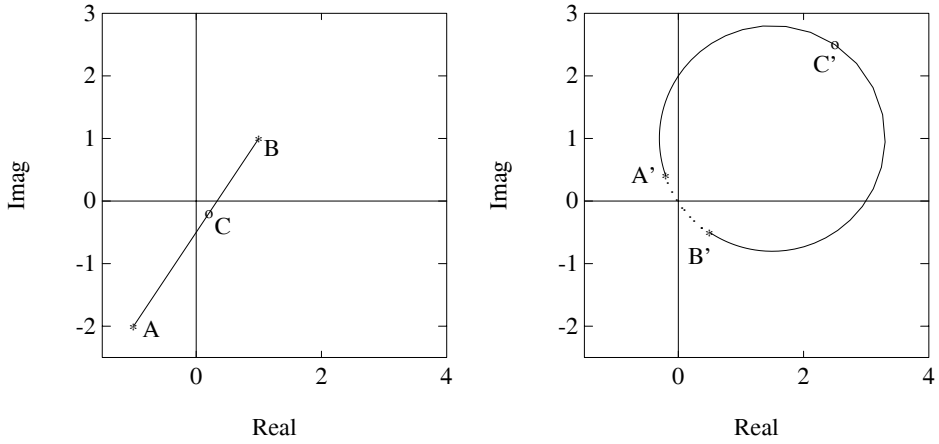

Figure 8.4. Line and inverse of line

To determine $\mathbf{\Delta}(j\omega)$ and $\mathbf{G}(j\omega)$ we note that the vertices of $\mathbf{N}(j\omega)$ and $\mathbf{D}(j\omega)$ correspond to the Kharitonov polynomials whereas the edges correspond to the Kharitonov segments. The set of points $\mathcal{K}_N(j\omega)$ are therefore the vertices of $\mathbf{N}(j\omega)$ and the four lines $\mathcal{S}_N(j\omega)$ are the edges of $\mathbf{N}(j\omega)$. $F_1(j\omega)\mathbf{N}(j\omega)$ is also a polygon with vertices $F_1(j\omega)\mathcal{K}_N(j\omega)$ and edges $F_1(j\omega)\mathcal{S}_N(j\omega)$. Similarly, $F_2(j\omega)\mathcal{K}_D(j\omega)$ and $F_2(j\omega)\mathcal{S}_D(j\omega)$ are the vertices and edges of the polygon $F_2(j\omega)\mathbf{D}(j\omega)$. The $j\omega$ image of the extremal systems $\mathbf{G}_{\mathrm{E}}(s)$ defined earlier exactly coincides with these

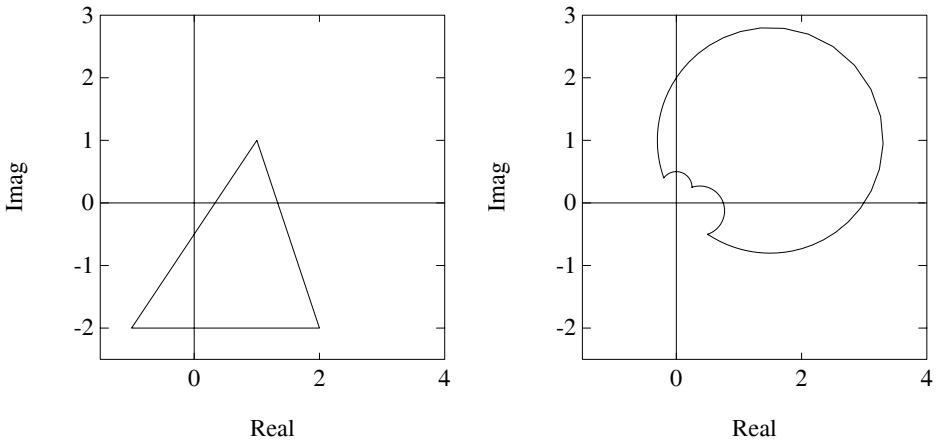

Figure 8.5. Polygon and the inverse of polygon

vertex-edge pairs. Let

$$(\mathbf{N}(s)\mathrm{x}\mathbf{D}(s))_{\mathrm{E}} := (\mathcal{K}_N(s)\mathrm{x}\mathcal{S}_D(s)) \cup (\mathcal{S}_N(s)\mathrm{x}\mathcal{K}_D(s)). \tag{8.11}$$

Recall that the *extremal systems* are

$$\mathbf{G}_{\mathrm{E}}(s) := \left\{ \frac{N(s)}{D(s)} \ : \ (N(s), D(s)) \in (\mathbf{N}(s)\mathrm{x}\mathbf{D}(s))_{\mathrm{E}} \right\} := \frac{\mathcal{K}_N(s)}{\mathcal{S}_D(s)} \cup \frac{\mathcal{S}_N(s)}{\mathcal{K}_D(s)} \tag{8.12}$$

and define

$$\mathbf{\Delta}_{\mathrm{E}}(s) := \{F_1(s)N(s) + F_2(s)D(s) \ : \ (N(s), D(s)) \in (\mathbf{N}(s)\mathrm{x}\mathbf{D}(s))_{\mathrm{E}}\}. \tag{8.13}$$

We can now state an important result regarding the boundary of image sets.

Theorem 8.2 (Boundary Generating Property)

$$\begin{aligned} &a) \quad \partial\mathbf{\Delta}(j\omega) \subset \mathbf{\Delta}_{\mathrm{E}}(j\omega) \\ &b) \quad \partial\mathbf{G}(j\omega) \subset \mathbf{G}_{\mathrm{E}}(j\omega) \end{aligned}$$

Proof. The proof of this theorem follows immediately from Lemma 8.1 and the observation regarding the vertices and edges of $\mathbf{N}(j\omega)$ and $\mathbf{D}(j\omega)$.

a) From Lemma 8.1,

$$\begin{aligned} \partial\mathbf{\Delta}(j\omega) &\subset (F_1(j\omega)\mathcal{K}_N(j\omega) + F_2(j\omega)\mathcal{S}_D(j\omega)) \\ &\quad \cup (F_1(j\omega)\mathcal{S}_N(j\omega) + F_2(j\omega)\mathcal{K}_D(j\omega)) \\ &= \mathbf{\Delta}_{\mathrm{E}}(j\omega) \quad (see (8.11) \text{ and } (8.13)). \end{aligned}$$

b)

$$\begin{aligned}\partial\mathbf{G}(j\omega) &\subset \left[\frac{\mathcal{K}_N(j\omega)}{\mathcal{S}_D(j\omega)} \cup \frac{\mathcal{S}_N(j\omega)}{\mathcal{K}_D(j\omega)}\right] \\ &= \mathbf{G}_{\mathrm{E}}(j\omega) \quad (\text{see } (8.12)).\end{aligned}$$

♣

Example 8.1. Consider the problem of determining the frequency template of the interval plant

$$G(s) = \frac{n(s)}{d(s)} = \frac{b_1 s + b_0}{a_2 s^2 + a_1 s + a_0}$$

where the parameters vary as follows:

$$a_0 \in [1,2], \quad a_1 \in [2,3], \quad a_2 \in [2,3], \quad b_0 \in [1,2], \quad b_1 \in [2,3].$$

The Kharitonov polynomials of $d(s)$ and $n(s)$ are:

$$\begin{aligned}K_d^1(s) &= 3s^2 + 2s + 1 \\ K_d^2(s) &= 3s^2 + 3s + 1 \\ K_d^3(s) &= 2s^2 + 2s + 2 \\ K_d^4(s) &= 2s^2 + 3s + 2\end{aligned}$$

and

$$\begin{aligned}K_n^1(s) &= 2s + 1 \\ K_n^2(s) &= 3s + 1 \\ K_n^3(s) &= 2s + 2 \\ K_n^4(s) &= 3s + 2.\end{aligned}$$

Thus, the boundary of the entire frequency domain template is obtained by the frequency evaluation of the following 32 systems:

$$\frac{K_n^i(s)}{\lambda K_d^j(s) + (1-\lambda) K_d^k(s)}, \quad \text{and} \quad \frac{\lambda K_n^j(s) + (1-\lambda) K_n^k(s)}{K_d^i(s)},$$

for

$$i = 1,2,3,4; \quad (j,k) \in \{(1,2),(1,3),(2,3),(3,4)\}.$$

Figure 8.6 shows the template $\mathbf{G}(j\omega)$ at $\omega = 1$.

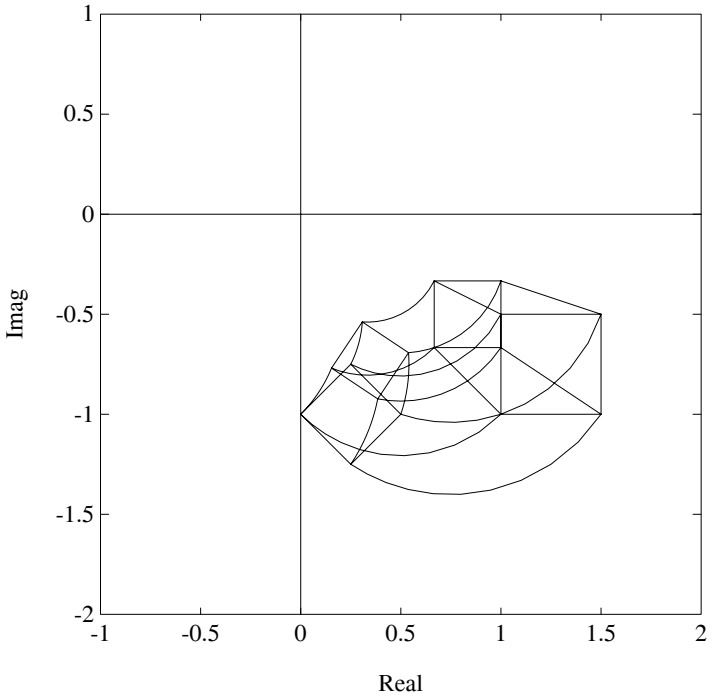

Figure 8.6. Frequency domain template $\mathbf{G}(j\omega)$ (Example 8.1)

Closed Loop Transfer Functions

Referring now to the control system in Figure 8.1, we consider the following transfer functions of interest in analysis and design problems:

$$\frac{y(s)}{u(s)} = G(s), \qquad \frac{u(s)}{e(s)} = F(s) \tag{8.14}$$

$$T^o(s) := \frac{y(s)}{e(s)} = F(s)G(s) \tag{8.15}$$

$$T^e(s) := \frac{e(s)}{r(s)} = \frac{1}{1 + F(s)G(s)} \tag{8.16}$$

$$T^u(s) := \frac{u(s)}{r(s)} = \frac{F(s)}{1 + F(s)G(s)} \tag{8.17}$$

$$T^y(s) := \frac{y(s)}{r(s)} = \frac{F(s)G(s)}{1 + F(s)G(s)}. \tag{8.18}$$

As $G(s)$ ranges over the uncertainty set $\mathbf{G}(s)$ the transfer functions $T^o(s)$, $T^y(s)$, $T^u(s)$, $T^e(s)$ range over corresponding uncertainty sets $\mathbf{T}^o(s)$, $\mathbf{T}^y(s)$, $\mathbf{T}^u(s)$, and $\mathbf{T}^e(s)$, respectively. In other words,

$$\mathbf{T}^o(s) := \{F(s)G(s) \ : \ G(s) \in \mathbf{G}(s)\} \tag{8.19}$$

$$\mathbf{T}^e(s) := \left\{ \frac{1}{1+F(s)G(s)} \ : \ G(s) \in \mathbf{G}(s) \right\} \tag{8.20}$$

$$\mathbf{T}^u(s) := \left\{ \frac{F(s)}{1+F(s)G(s)} \ : \ G(s) \in \mathbf{G}(s) \right\} \tag{8.21}$$

$$\mathbf{T}^y(s) := \left\{ \frac{F(s)G(s)}{1+F(s)G(s)} \ : \ G(s) \in \mathbf{G}(s) \right\}. \tag{8.22}$$

We will now show that the boundary generating property of the extremal subsets shown in Theorem 8.2 carries over to each of the system transfer functions listed above. In fact, we will show that the boundary of the image set at $s = j\omega$, the Nyquist plot and Bode plot boundaries of each of the above sets are all generated by the subset $\mathbf{G}_{\rm E}(s)$. Introduce the subsets of (8.19) - (8.22) obtained by replacing $\mathbf{G}(s)$ by $\mathbf{G}_{\rm E}(s)$:

$$\mathbf{T}^o_{\rm E}(s) := \{F(s)G(s) \ : \ G(s) \in \mathbf{G}_{\rm E}(s)\} \tag{8.23}$$

$$\mathbf{T}^e_{\rm E}(s) := \left\{ \frac{1}{1+F(s)G(s)} \ : \ G(s) \in \mathbf{G}_{\rm E}(s) \right\} \tag{8.24}$$

$$\mathbf{T}^u_{\rm E}(s) := \left\{ \frac{F(s)}{1+F(s)G(s)} \ : \ G(s) \in \mathbf{G}_{\rm E}(s) \right\} \tag{8.25}$$

$$\mathbf{T}^y_{\rm E}(s) := \left\{ \frac{F(s)G(s)}{1+F(s)G(s)} \ : \ G(s) \in \mathbf{G}_{\rm E}(s) \right\}. \tag{8.26}$$

The main result can now be stated.

Theorem 8.3 *For every $\omega \geq 0$,*

$$\begin{array}{ll} (a) & \partial \mathbf{T}^o(j\omega) \subset \mathbf{T}^o_{\rm E}(j\omega) \\ (b) & \partial \mathbf{T}^e(j\omega) \subset \mathbf{T}^e_{\rm E}(j\omega) \\ (c) & \partial \mathbf{T}^u(j\omega) \subset \mathbf{T}^u_{\rm E}(j\omega) \\ (d) & \partial \mathbf{T}^y(j\omega) \subset \mathbf{T}^y_{\rm E}(j\omega) \end{array}$$

The proof will require the following technical lemma.

Lemma 8.2 *Let $\mathcal{D}$ be a closed set in the complex plane with $0 \notin \mathcal{D}$. Then*

$$\partial \left(\frac{1}{\mathcal{D}} \right) = \frac{1}{\partial \mathcal{D}}. \tag{8.27}$$

Proof. Let $\frac{1}{d_0} \in \partial(\frac{1}{\mathcal{D}})$, then there exists an open disc such that $\left| \frac{1}{d} - \frac{1}{d_0} \right| < \epsilon$ for some d such that $\frac{1}{d} \notin \frac{1}{\mathcal{D}}$. This implies that $d \notin \mathcal{D}$ but $d_0 \in \mathcal{D}$. By the continuity of

the mapping with respect to d at d_0, it follows that $\frac{1}{d_0} \in \frac{1}{\partial \mathcal{D}}$. Conversely, suppose that $d_0 \in \partial\mathcal{D}$, equivalently $\frac{1}{d_0} \in \frac{1}{\partial \mathcal{D}}$. Then there exists an open disc such that $|d - d_0| < \epsilon$ for some $d \notin \mathcal{D}$. This implies that $\frac{1}{d} \notin \frac{1}{\mathcal{D}}$ while $\frac{1}{d_0} \in \frac{1}{\mathcal{D}}$. Again, by the continuity of the mapping with respect to d at d_0, we have $\frac{1}{d_0} \in \partial(\frac{1}{\mathcal{D}})$. ♣

Proof of Theorem 8.3

(a)

$$\begin{aligned}\partial \mathbf{T}^o(j\omega) &= \partial(\mathbf{G}(j\omega)F(j\omega)) = F(j\omega)\partial\mathbf{G}(j\omega) \\ &\subset F(j\omega)\mathbf{G}_{\mathrm{E}}(j\omega) = \mathbf{T}_{\mathrm{E}}(j\omega).\end{aligned}$$

(b) From Lemma 8.2,

$$\begin{aligned}\partial \mathbf{T}^e(j\omega) &= \partial\left(\frac{1}{1+\mathbf{G}(j\omega)F(j\omega)}\right) = \frac{1}{\partial(1+\mathbf{G}(j\omega)F(j\omega))} \\ &= \frac{1}{1+\partial(\mathbf{G}(j\omega)F(j\omega))}.\end{aligned}$$

Since $\partial(\mathbf{G}(j\omega)F(j\omega)) \subset \mathbf{G}_{\mathrm{E}}(j\omega)F(j\omega)$, we have $\partial\mathbf{T}^e(j\omega) \subset \mathbf{T}^e_{\mathrm{E}}(j\omega)$.

(c) Since $\mathbf{T}^u(j\omega) = F(j\omega)\mathbf{T}^e(j\omega)$ with a fixed $F(j\omega)$ for a fixed ω, the property shown in (c) carries over directly. Thus, $\partial\mathbf{T}^u(j\omega) \subset \mathbf{T}^u_{\mathrm{E}}(j\omega)$.

(d)

$$\begin{aligned}\partial \mathbf{T}^y(j\omega) &= \partial\left(\frac{1}{1+\frac{1}{F(j\omega)\mathbf{G}(j\omega)}}\right) = \frac{1}{\partial\left(1+\frac{1}{F(j\omega)\mathbf{G}(j\omega)}\right)} \\ &= \frac{1}{1+\frac{1}{F(j\omega)\partial\mathbf{G}(j\omega)}} \\ &\subset \frac{1}{1+\frac{1}{F(j\omega)\mathbf{G}_{\mathrm{E}}(j\omega)}} \\ &= \mathbf{T}^y_{\mathrm{E}}(j\omega)\end{aligned}$$

♣

Remark 8.1. This result shows that at every $\omega \geq 0$, the boundary of the image set of each transfer function in (8.19) - (8.22) is contained in the corresponding image set of the extremal systems. We point out that in the definition of the

interval plant $\mathbf{G}(s)$ we assumed that the numerator and denominator parameters were independent. This assumption obviously does not hold any longer when we deal with say, $\mathbf{T}^y(s)$ where the numerator and denominator depend on some common parameters. It is therefore useful to know that the boundary generating property of the set $\mathbf{G}_{\mathrm{E}}(s)$ carries over nevertheless. In a later section we will show that the boundary generating property of the set $\mathbf{G}_{\mathrm{E}}(s)$ will hold much more generally.

Example 8.2. Consider the system given in Example 8.1. Let us assume that $F(s) = 1$ and that we wish to calculate $\mathbf{T}^y(j\omega)$.

$$\mathbf{T}^y(s) = \left\{ \frac{G(s)}{1+G(s)} : G(s) \in \mathbf{G}(s) \right\}.$$

For this example, we have

$$T^y(s) = \frac{b_1 s + b_0}{a_2 s^2 + (a_1 + b_1)s + (a_0 + b_0)}$$

where

$$a_0 \in [1,2], \quad a_1 \in [2,3], \quad a_2 \in [2,3], \quad b_0 \in [1,2], \quad b_1 \in [2,3].$$

The denominator and numerator polynomials are dependent on some of the same perturbing parameters. However, Theorem 8.3 handles this dependency. Since $\partial \mathbf{T}^y(j\omega) \subset \mathbf{T}^y_{\mathrm{E}}(j\omega)$, it is enough to construct the following template:

$$\mathbf{T}^y_{\mathrm{E}}(j\omega) = \left\{ \frac{G(j\omega)}{1+G(j\omega)} : G(j\omega) \in \mathbf{G}_{\mathrm{E}}(j\omega) \right\}.$$

In other words, we simply replace $\mathbf{G}(s)$ by $\mathbf{G}_E(s)$ in $\mathbf{T}^y$. Thus we need to construct the image of the following transfer functions for $\lambda \in [0,1]$:

$$\frac{K^i_n(j\omega)}{\lambda K^k_d(j\omega) + (1-\lambda)K^l_d(j\omega) + K^i_n(j\omega)}$$

and

$$\frac{\lambda K^k_n(j\omega) + (1-\lambda)K^l_n(j\omega)}{\lambda K^k_n(j\omega) + (1-\lambda)K^l_n(j\omega) + K^i_d(j\omega)}$$

for $i = 1,2,3,4$ and $(k,l) \in \{(1,2),(1,3),(2,3),(3,4)\}$. The sets of Kharitonov polynomials corresponding to the denominator and numerator polynomials are defined in Example 8.1. The frequency domain template at $\omega = 1$ is shown in Figure 8.7.

8.4 NYQUIST, BODE, AND NICHOLS ENVELOPES

In the previous section we established that at a fixed frequency the image set template of various transfer function set can be constructed from the corresponding extremal transfer function set $\mathbf{G}_{\mathrm{E}}(s)$. In control system design it is important to

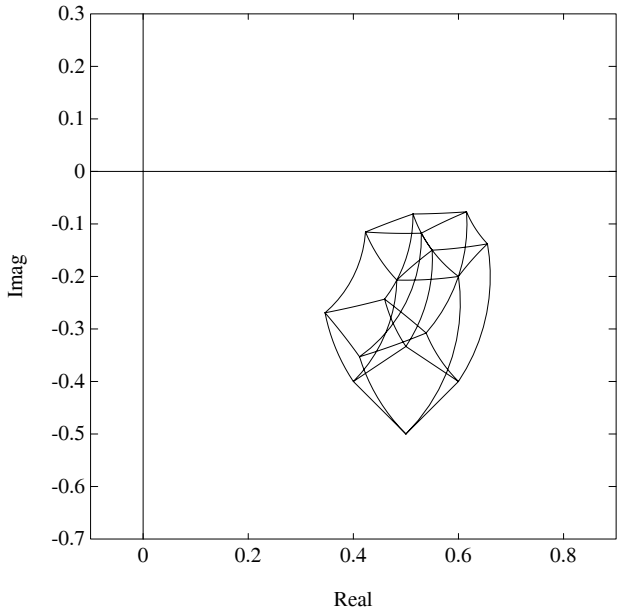

Figure 8.7. Frequency domain template $\mathbf{T}^y(j\omega)$ (Example 8.2)

see the behaviour of these transfer function families for all frequency. Denote the Nyquist plot of the family $\mathbf{G}(s)$ as

$$\mathbf{G} = \cup_{0 \leq \omega < \infty} \mathbf{G}(j\omega). \tag{8.28}$$

The boundary of $\mathbf{G}$ is the Nyquist envelope of $\mathbf{G}$. Similarly, the Nyquist plots of $\mathbf{T}^o(s)$, $\mathbf{T}^e(s)$, $\mathbf{T}^u(s)$, and $\mathbf{T}^y(s)$ are denoted respectively by $\mathbf{T}^o$, $\mathbf{T}^e$, $\mathbf{T}^u$, and $\mathbf{T}^y$. From the boundary property of Theorem 8.3, it follows that the envelopes of these Nyquist plots are generated by the extremal systems.

Theorem 8.4 (Nyquist Envelope)
The Nyquist plots of each of the transfer function sets $\mathbf{T}^o(s)$, $\mathbf{T}^y(s)$, $\mathbf{T}^u(s)$, *and* $\mathbf{T}^e(s)$ *are bounded by their corresponding extremal subsets:*

$$\begin{aligned}
&(a) \quad \partial\mathbf{G} \subset \mathbf{G}_{\mathrm{E}} \\
&(b) \quad \partial\mathbf{T}^o \subset \mathbf{T}^o_{\mathrm{E}} \\
&(c) \quad \partial\mathbf{T}^y \subset \mathbf{T}^y_{\mathrm{E}} \\
&(d) \quad \partial\mathbf{T}^u \subset \mathbf{T}^u_{\mathrm{E}} \\
&(e) \quad \partial\mathbf{T}^e \subset \mathbf{T}^e_{\mathrm{E}}.
\end{aligned} \tag{8.29}$$

The Bode envelopes of each of the system transfer functions $\mathbf{G}(s)$, $\mathbf{T}^o(s)$, $\mathbf{T}^e(s)$, $\mathbf{T}^u(s)$, and $\mathbf{T}^y(s)$ can also be constructed if we can determine the maximum and minimum values of the magnitude and phase of the family of systems at each frequency. From the boundary relations given in Theorem 8.3, it again follows that these maximum and minimum values occur over the subset $\mathbf{G}_{\mathrm{E}}(s)$. This leads us to the following result.

Theorem 8.5 (Bode Envelope)
The Bode magnitude and phase envelopes of each of the transfer function sets $\mathbf{G}(s)$, $\mathbf{T}^o(s)$, $\mathbf{T}^e(s)$, $\mathbf{T}^u(s)$, $\mathbf{T}^y(s)$ *are generated respectively by the extremal subsets,* $\mathbf{G}_{\mathrm{E}}(s)$, $\mathbf{T}^o_{\mathrm{E}}(s)$, $\mathbf{T}^e_{\mathrm{E}}(s)$, $\mathbf{T}^u_{\mathrm{E}}(s)$, $\mathbf{T}^y_{\mathrm{E}}(s)$.

It is instructive to interpret this result from the geometric point of view. Consider the Bode plot of the interval family $\mathbf{G}(s)$. For a fixed ω^*, the image of the interval transfer function is the quotient of two convex polygons in the complex plane where the polygons represent the images of the numerator and denominator polynomial families. This is depicted in Figure 8.8.

From Figure 8.8(a) and (b), we can see that the maximum and minimum magnitudes of $\mathbf{G}(j\omega^*)$ occur on one of the vertex-segment combinations of these polygons. Since the parameters in the numerator and denominator are independent we have:

$$\text{(a)} \qquad \max \left| \frac{\mathbf{N}(j\omega^*)}{\mathbf{D}(j\omega^*)} \right| = \frac{\max |\mathbf{N}(j\omega^*)|}{\min |\mathbf{D}(j\omega^*)|}$$

$$\text{(b)} \qquad \min \left| \frac{\mathbf{N}(j\omega^*)}{\mathbf{D}(j\omega^*)} \right| = \frac{\min |\mathbf{N}(j\omega^*)|}{\max |\mathbf{D}(j\omega^*)|}.$$

While the maximum magnitude always occurs at a vertex the minimum can occur on an edge. The maximum and minimum points will generate the extreme points of the Bode magnitude envelope at the frequency ω^*. On the other hand, as shown in Figure 8.8(c) and (d), the extreme points on the phase envelope are always generated by vertex-vertex pairs:

$$\text{(c)} \qquad \max \arg \frac{\mathbf{N}(j\omega^*)}{\mathbf{D}(j\omega^*)} = \max \arg \mathbf{N}(j\omega^*) - \min \arg \mathbf{D}(j\omega^*)$$

$$\text{(d)} \qquad \min \arg \frac{\mathbf{N}(j\omega^*)}{\mathbf{D}(j\omega^*)} = \min \arg \mathbf{N}(j\omega^*) - \max \arg \mathbf{D}(j\omega^*).$$

The relations given in the Theorem above are useful in constructing the Bode magnitude and phase envelopes as well as Nyquist envelopes. In classical control design techniques, the Nichols Chart is also a popular computational tool. For a fixed transfer function, the Nichols Chart is a plot of the magnitude versus the phase with frequency as a running parameter. When a family of parametrized systems is involved, we get at each frequency a *magnitude-phase template.* When this template is swept over all frequencies, we get the Nichols Envelope of the family. By using

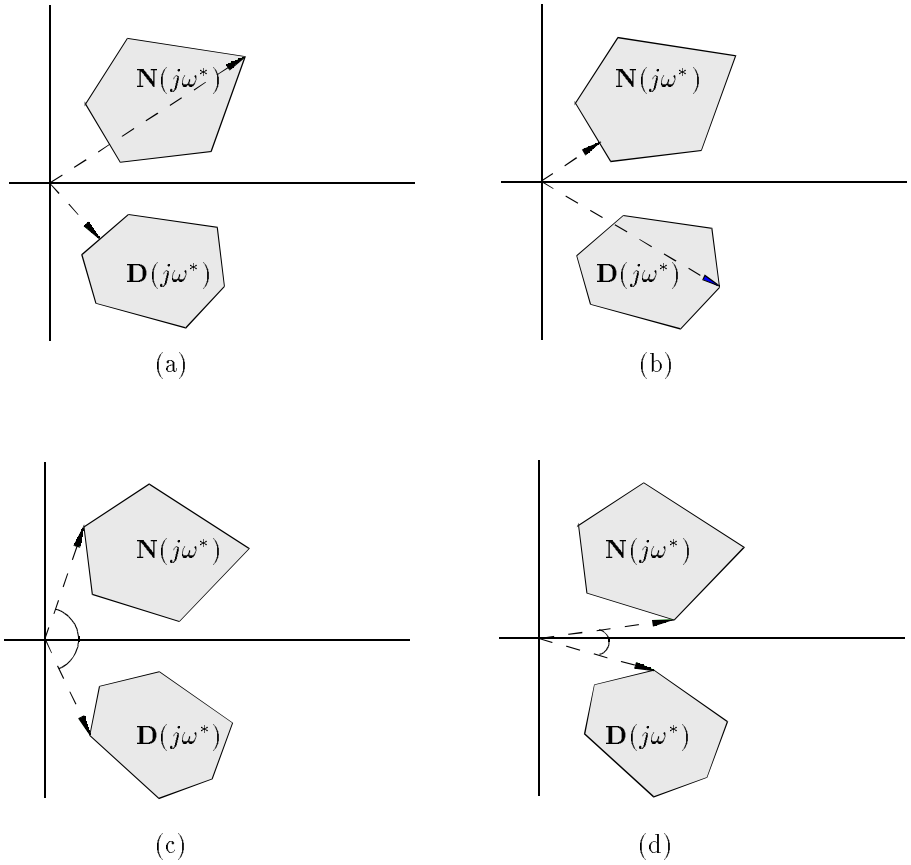

Figure 8.8. Extremal magnitude and phase of $\mathbf{N}(j\omega^*)$ and $\mathbf{D}(j\omega^*)$

the boundary property of Theorem 8.3 it can be seen that the Nichols Envelope is also generated by the extremal systems.

Theorem 8.6 (Nichols Envelope)
The Nichols Envelope of each of the transfer function sets $\mathbf{G}(s)$, $\mathbf{T}^o(s)$, $\mathbf{T}^e(s)$, $\mathbf{T}^u(s)$, $\mathbf{T}^y(s)$ *are generated respectively by the extremal subsets,* $\mathbf{G}_{\mathrm{E}}(s)$, $\mathbf{T}^o_{\mathrm{E}}(s)$, $\mathbf{T}^e_{\mathrm{E}}(s)$, $\mathbf{T}^u_{\mathrm{E}}(s)$, $\mathbf{T}^y_{\mathrm{E}}(s)$.

The Nichols template is obtained by mapping the points of the Nyquist plane (see Figure 8.9) into the Nichols plane (see Figure 8.10). This gives the exact Nichols template. The Nichols envelope can also be generated approximately from the Bode magnitude and phase envelopes of the family. At each frequency we draw

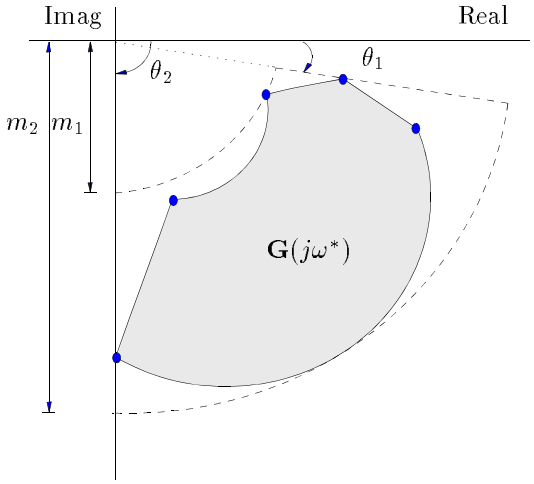

Figure 8.9. A Nyquist template

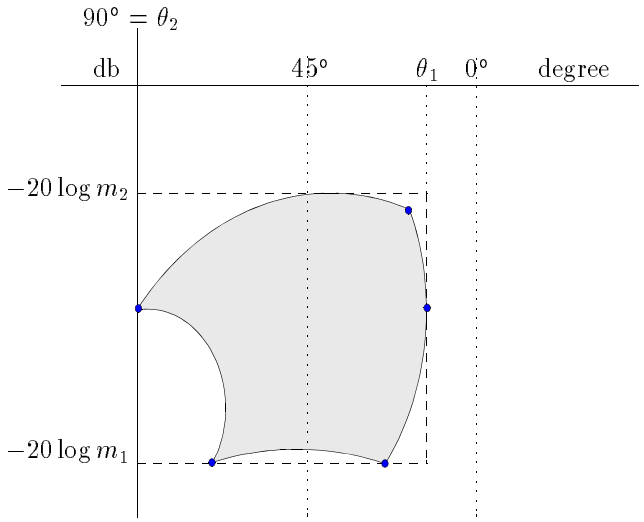

Figure 8.10. A Nichols template

a rectangle in the magnitude-phase plane (Nichols plane). The dashed rectangle shown in Figure 8.10 corresponds to the magnitude and phase ranges obtained from the Bode envelopes. When these overbounded images of $\mathbf{G}(j\omega)$ templates are swept over frequency, we obtain the approximate Nichols envelope which contains the actual envelope. We illustrate these computations with an example.

Example 8.3. Consider the plant and controller

$$G(s) = \frac{b_1 s + b_0}{a_2 s^2 + a_1 s + a_0} \qquad C(s) = \frac{s^2 + 2s + 1}{s^4 + 2s^3 + 2s^2 + s}$$

where the plant parameters vary as

$$b_1 \in [0.1, 0.2], \quad b_0 \in [0.9, 1.1]$$
$$a_2 \in [0.9, 1.0], \quad a_1 \in [1.8, 2.0], \quad a_0 \in [1.9, 2.1].$$

Figures 8.11, 8.12, and 8.13 show the frequency domain plots for this example.

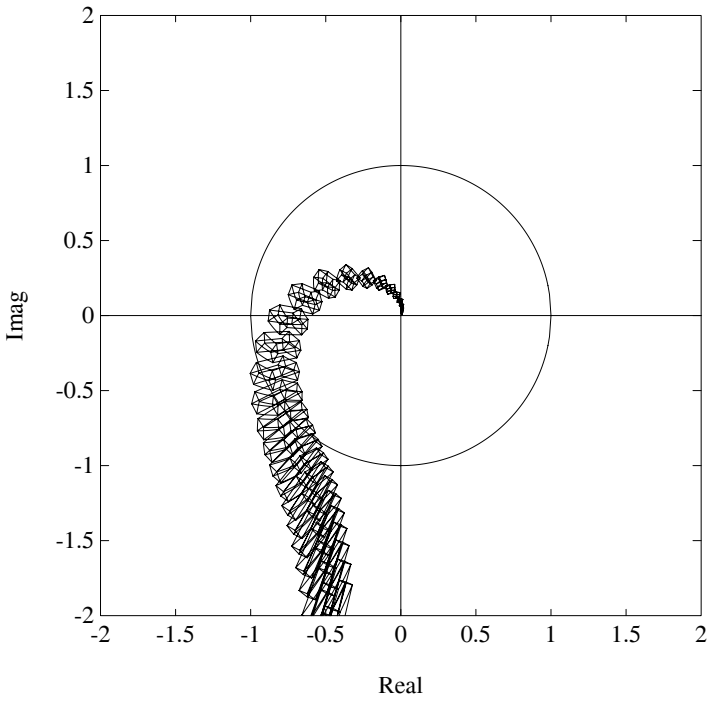

Figure 8.11. Nyquist templates (Example 8.3)

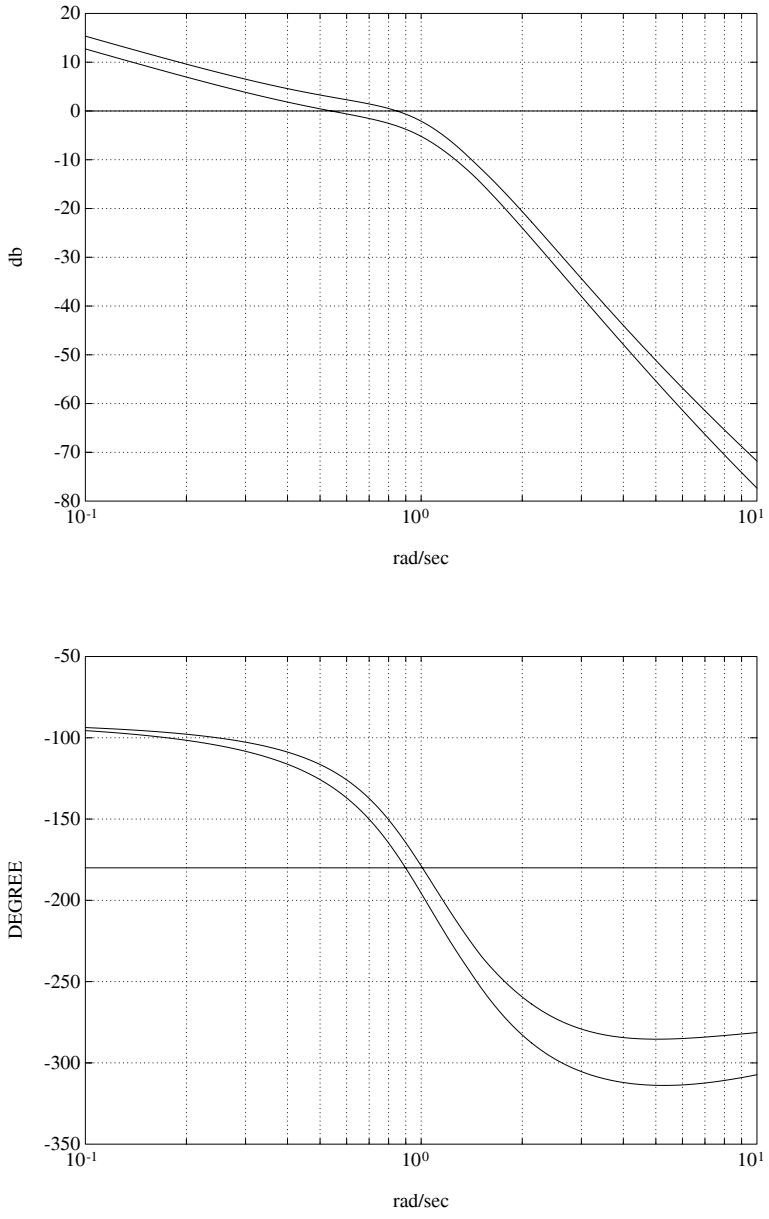

Figure 8.12. Bode envelopes (Example 8.3)

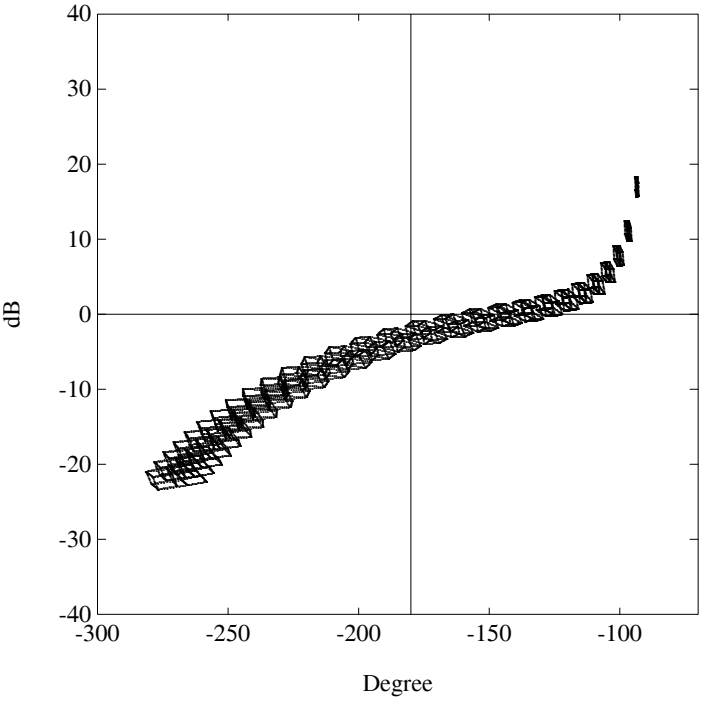

Figure 8.13. Nichols envelope (Example 8.3)

Conservatism of the Envelopes

For a fixed system, all of the above three frequency plots provide the same information on the system. However, for the case of a parametrized family of systems, the situation is quite different. The Nyquist and Nichols plots of a fixed system can be regarded as a string in the Nyquist or Nichols plane. For a parametrized family of systems, the Nyquist or Nichols plots therefore consists of a family of strings. However, the envelope of the plot is, in general, not a string that belongs to the family. In other words, there is no system in the family which generates the entire boundary of the envelope itself. On the other hand, every point on the boundary of the envelope has a string passing through it as shown in Figures 8.14 and 8.15.

The Bode envelopes in fact correspond to an overbound of the image of the complex plane set $\mathbf{G}(j\omega)$ at each frequency ω. Considering Figure 8.16, we also see that each point on the boundaries of the envelopes came from a true member system of the family. From the Bode envelopes, we notice that the smallest gain margin of the family is K. However, the member system passing through the "•" point in the magnitude plot does not correspond to the phase crossover point "•"

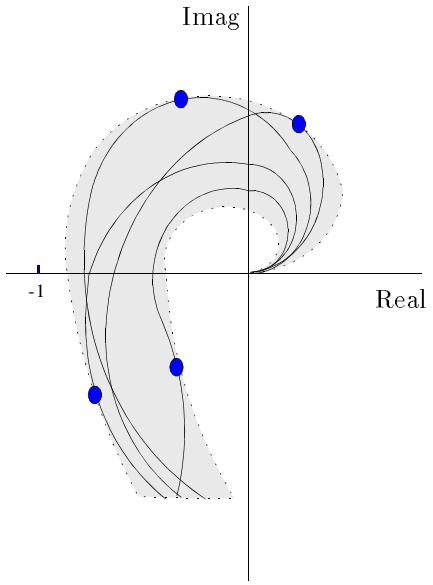

Figure 8.14. Nyquist envelope and Nyquist plots of individual member systems

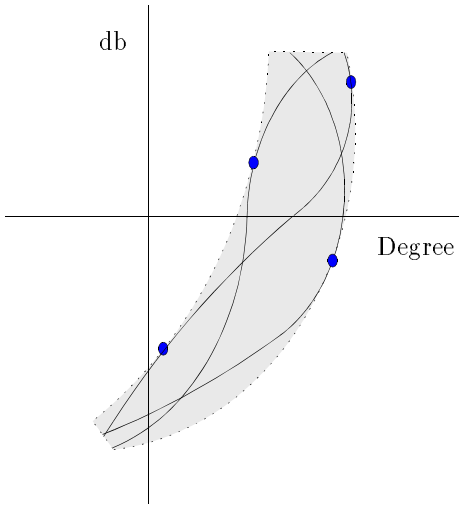

Figure 8.15. Nichols envelope and Nichols plots of individual member systems

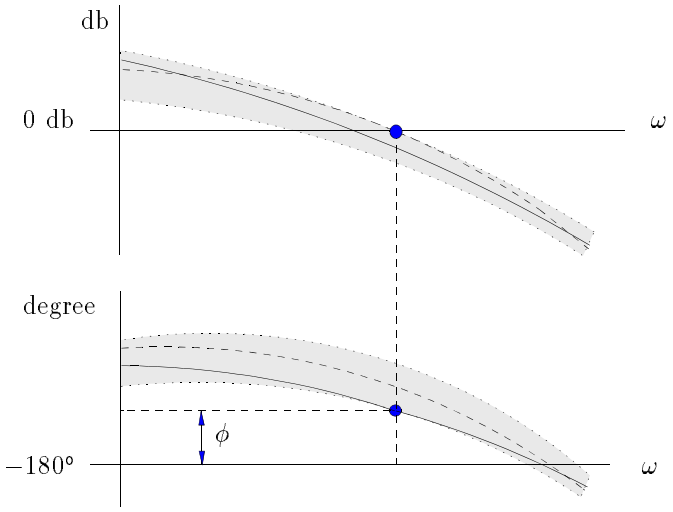

Figure 8.16. Bode envelopes and guaranteed phase margin

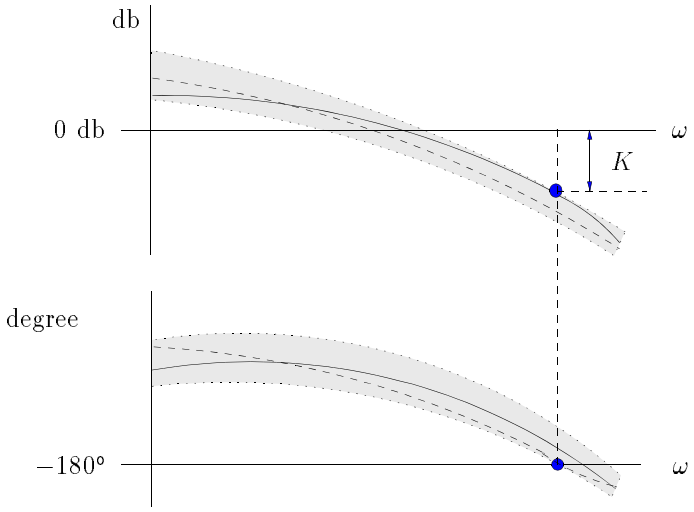

Figure 8.17. Bode envelopes and guaranteed gain margin

in the phase plot. Due to this phenomena, the true smallest gain margin might be bigger than K. A similar argument can be made for the case of the smallest phase margin (see Figure 8.17). This is because of the *independent* evaluation of the magnitude and phase envelopes of the family. In other words, despite the fact that each point on the boundaries of the Bode magnitude and phase envelopes, comes from some parameter in the family, the latter envelopes taken jointly, represent only the approximate set which corresponds to the dashed box in Figure 8.10 and equivalently, the dashed portion of the disc in Figure 8.9. Therefore, the smallest gain and phase margins read from the Bode envelopes would be conservative, with the degree of conservatism depending upon how big the actual image inside the dashed box is (see Figure 8.10).

Remark 8.2. The above boundary results remain valid if $F_i(s)$ are complex functions rather than real polynomials. This is useful in applications. For example, in systems containing time-delay $F_i(s)$ could contain terms such as e^{-Ts}. Also many robust performance problems reduce to verifying robust stability under real parameter perturbations using complex compensators.

8.5 EXTREMAL STABILITY MARGINS

In this section, we deal with the calculation of guaranteed stability margins. We will first consider the gain and phase margins at the loop breaking point "m" shown in Figure 8.18. When $G(s)$ contains parameter uncertainty the worst case values of

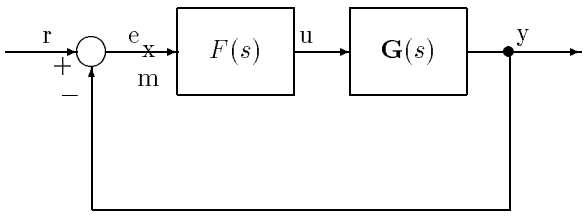

Figure 8.18. A unity feedback system

gain and phase margins over the parameter uncertainty set are important measures of robust performance. We show that these worst case margins in fact occur over the subset of extremal plants $\mathbf{G}_{\mathrm{E}}(s)$.

8.5.1 Guaranteed Gain and Phase Margins

Suppose that $F(s)$ robustly stabilizes the family $\mathbf{G}(s)$. The gain margin of the system for a fixed $G(s) \in \mathbf{G}(s)$ is defined to be the smallest value K_G for which

$$(1+K)F_1(s)N(s) + F_2(s)D(s)$$

remains stable for all $K \in [0, K_G)$. Similarly, the phase margin of the system for a fixed $G(s) \in \mathbf{G}(s)$ is defined to be the smallest value θ_G for which

$$e^{j\theta}F_1(s)N(s) + F_2(s)D(s)$$

remains stable for all $\theta \in [0, \theta_G)$. The worst case gain and phase margins are:

$$K^* := \inf_{G(s)\in\mathbf{G}(s)} K_G \qquad \theta^* := \inf_{G(s)\in\mathbf{G}(s)} \theta_G. \tag{8.30}$$

Theorem 8.7 (Extremal Gain and Phase Margin)

I)

$$K^* = \inf_{G(s)\in\mathbf{G}_{\mathrm{E}}(s)} K_G, \qquad \theta^* = \inf_{G(s)\in\mathbf{G}_{\mathrm{E}}(s)} \theta_G.$$

II) If $F_i(s)$ are real and satisfy the vertex conditions specified in part II of GKT, then we have

$$K^* = \inf_{G(s)\in\mathbf{G}_{\mathrm{K}}(s)} K_G$$

The proof of this theorem readily follows from the fact that $\mathbf{\Delta}(j\omega)$ and $\mathbf{\Delta}_{\mathrm{E}}(j\omega)$ share identical boundaries. Moreover, when $F_i(s)$ satisfy the vertex conditions the proof follows from the fact that $\mathbf{\Delta}(s)$ is stable if and only if $\mathbf{\Delta}_{\mathrm{K}}(s)$ is stable.

8.5.2 Worst Case Parametric Stability Margin

We now consider the worst case parametric stability margin. We assume as before that $F(s)$ robustly stabilizes $\mathbf{G}(s)$. The parameter $\mathbf{p}$ of dimension t consists of the coefficients of $\mathbf{N}(s)$ and $\mathbf{D}(s)$ and varies in the hypercube $\mathbf{\Pi}$. We will rewrite $\delta(s)$ in (8.5) as $\delta(s, \mathbf{p})$ to emphasize its dependence on the parameter $\mathbf{p}$. Let $\mathbf{\Pi}_{\mathrm{E}}$ denote the parameter subset of $\mathbf{\Pi}$ corresponding to the extremal systems $\mathbf{G}_{\mathrm{E}}(s)$. Let $\mathbf{\Pi}_{\mathrm{K}}$ denote the parameter subset of $\mathbf{\Pi}$ corresponding to the extremal systems $\mathbf{G}_{\mathrm{K}}(s)$.

Let $\|\cdot\|$ denote any norm in $\mathbb{R}^t$ and let $\mathcal{P}_u$ denote the set of points $\mathbf{u}$ in $\mathbb{R}^t$ for which $\delta(s, \mathbf{u})$ is unstable or loses degree (relative to its generic degree over $\mathbf{\Pi}$). Let

$$\rho(\mathbf{p}) = \inf_{\mathbf{u}\in\mathcal{P}_u} \|\mathbf{p} - \mathbf{u}\|_p$$

denote the radius of the stability ball (measured in the norm $\|\cdot\|$) and centered at the point $\mathbf{p}$. This number serves as the stability margin associated with the point $\mathbf{p}$ and indicates its distance from instability. If the box $\mathbf{\Pi}$ is stable we can associate

a stability margin, denoted $\rho(\mathbf{p})$, with each point in $\mathbf{\Pi}$. A natural question to ask then is: What is the worst case value of the parametric stability margin over $\mathbf{\Pi}$ and what is the point where it occurs? An answer to this question gives an indication of how close one can get to instability over the box $\mathbf{\Pi}$.

Define a mapping from $\mathbf{\Pi}$ to the set of all positive real numbers:

$$\begin{aligned} \mathbf{\Pi} &\xrightarrow{\rho} \mathcal{R}^+\backslash\{0\} \\ \mathbf{p} &\longrightarrow \rho(\mathbf{p}) \end{aligned}$$

Our question stated in terms of functions is: Has the function $\rho(\mathbf{p})$ a minimum and is there a precise point in $\mathbf{\Pi}$ where it is reached? The answer is provided by the following theorem:

Theorem 8.8 (Extremal Parametric Stability Margin)

I) The minimum value over $\mathbf{\Pi}$ *of* $\rho(\mathbf{p})$ *is reached at a point on the extremal set* $\mathbf{\Pi}_{\rm E}$.

II) If $F_i(s)$ *satisfy the vertex conditions, the minimum value of* $\rho(\mathbf{p})$ *is reached at a point on the extremal set* $\mathbf{\Pi}_{\rm K}$.

Proof. The theorem amounts to proving that

$$\inf_{\mathbf{p}\in\mathbf{\Pi}} \rho(\mathbf{p}) = \inf_{\mathbf{p}\in\mathbf{\Pi}_{\rm E}} \rho(\mathbf{p}).$$

Since $\mathbf{\Delta}(j\omega)$ and $\mathbf{\Delta}_E(j\omega)$ have the same boundary,

$$\begin{aligned} \inf_{\mathbf{p}\in\mathbf{\Pi}} \rho(\mathbf{p}) &= \inf_{\mathbf{p}\in\mathbf{\Pi}} \inf_{\mathbf{u}\in\mathcal{P}_u} \|\mathbf{p}-\mathbf{u}\|_p \\ &= \inf\{\|\mathbf{a}\| \ : \ \delta(j\omega, \mathbf{p}+\mathbf{a}) = 0, \mathbf{p}\in\mathbf{\Pi}, \omega\in[-\infty,+\infty]\} \\ &= \inf\{\|\mathbf{a}\| \ : \ \delta(j\omega, \mathbf{p}+\mathbf{a}) = 0, \mathbf{p}\in\mathbf{\Pi}_{\rm E}, \omega\in[-\infty,+\infty]\} \\ &= \inf_{\mathbf{p}\in\mathbf{\Pi}_{\rm E}} \inf_{\mathbf{u}\in\mathcal{P}_u} \|\mathbf{p}-\mathbf{u}\|_p \\ &= \inf_{\mathbf{p}\in\mathbf{\Pi}_{\rm E}} \rho(\mathbf{p}). \end{aligned} \tag{8.31}$$

The proof of part II is identical. ♣

Example 8.4. Consider the unity feedback control system with

$$G(s) = \frac{a_1 s + a_0}{b_2 s^2 + b_1 s + b_0}$$

and

$$F(s) = \frac{s^2 + 2s + 1}{s^4 + 2s^3 + 2s^2 + s}$$

where

$$a_1 \in [0.15-\epsilon, 0.15+\epsilon], \quad a_0 \in [1-\epsilon, 1+\epsilon],$$
$$b_2 \in [0.95-\epsilon, 0.95+\epsilon], \quad b_1 \in [1.9-\epsilon, 1.9+\epsilon], \quad b_0 \in [2-\epsilon, 2+\epsilon].$$

We wish to find the largest excursion of parameters allowed or equivalently the maximum value of ϵ for which closed loop stability is preserved. The image set plot at $\epsilon = 0.128$, shown in Figure 8.19, reveals that the phase difference reaches 180° at $\epsilon \approx 0.128$ (Figure 8.20). It is clear that any value of ϵ smaller than 0.128 results in smaller image sets than the ones shown in Figure 8.19. Moreover, if we sweep the frequency the connected image sets will form an envelope which does not contain the origin for $\epsilon = 0.128$. Therefore, an envelope corresponding to any value of ϵ smaller than 0.128 cannot contain the origin. Thus, we conclude that the feedback system remains stable under the perturbations bounded by this maximum value of ϵ.

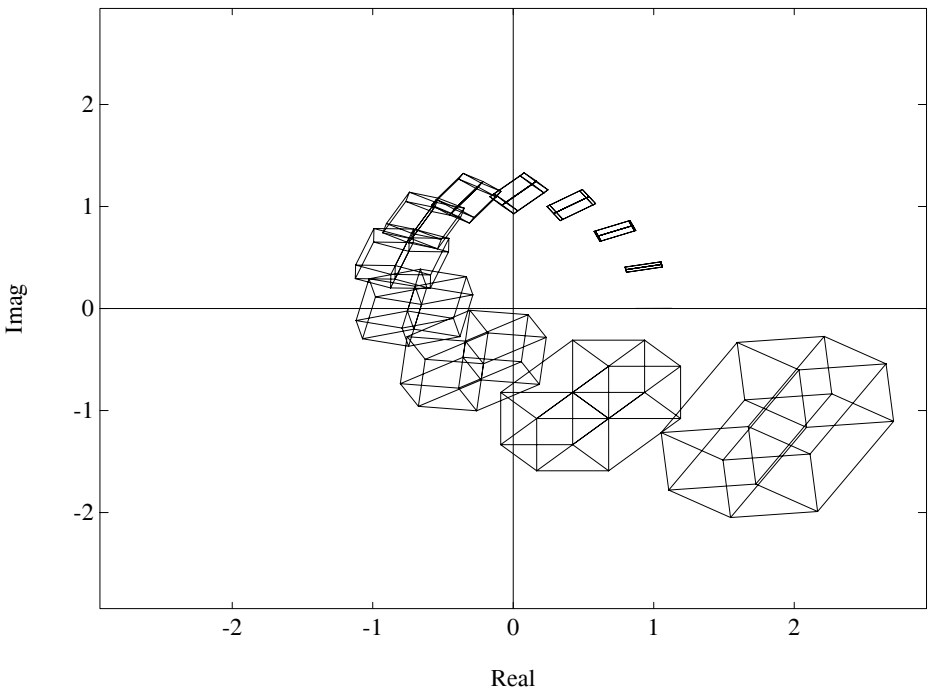

Figure 8.19. Image set plot at $\epsilon = 0.128$ (Example 8.4)

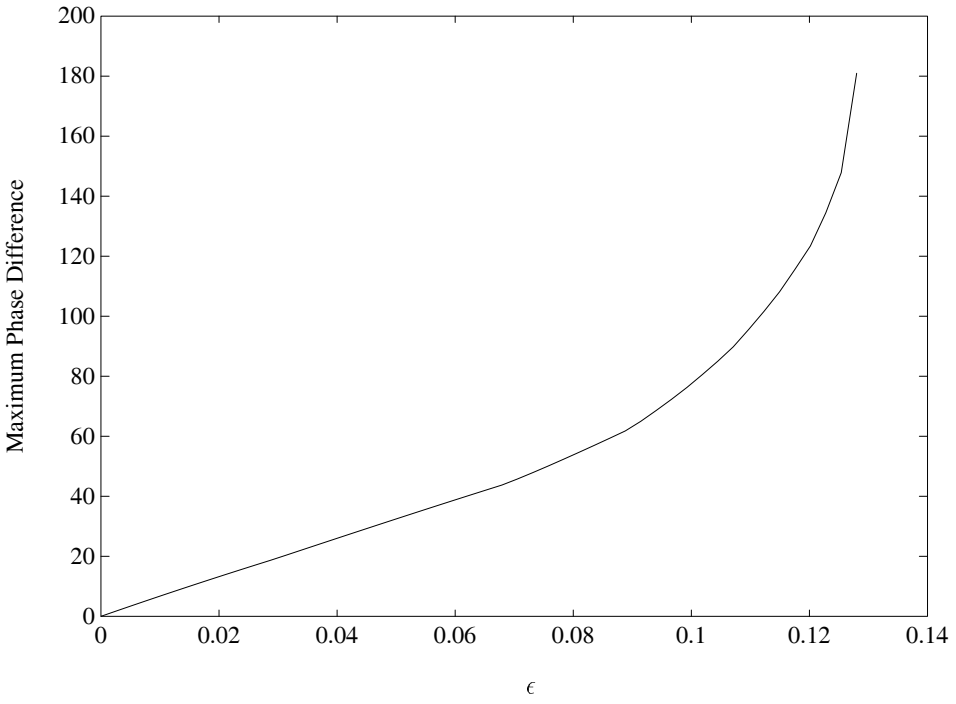

Figure 8.20. Phase plot (Example 8.4)

8.6 LINEAR INTERVAL CONTROL SYSTEMS

The results given so far in this chapter assume that $\mathbf{G}(s)$ is an interval plant, namely the ratio of interval polynomials. Each of the results given shows that a particular calculation involving $\mathbf{G}(\cdot)$ can be replaced by the corresponding calculation over the one parameter subsets $\mathbf{G}_{\mathrm{E}}(\cdot)$. This sort of simplification actually carries over to the more general class of *linear interval systems* $\mathbf{G}(s)$ defined below. Instead of repeating all the previous results, we show in this section how to construct the extremal subsets $\mathbf{G}_{\mathrm{E}}(s)$ and leave the details of the proofs to the reader.

We still consider the unity feedback system shown in Figure 8.1 with

$$F(s) := \frac{F_1(s)}{F_2(s)}, \qquad G(s) := \frac{N(s)}{D(s)}. \tag{8.32}$$

We suppose that $F(s)$ is fixed, $G(s)$ is subject to parametric uncertainty and is now

of the form

$$N(s) := L_1(s)A_1(s) + L_2(s)A_2(s) + \cdots + L_u(s)A_u(s)$$
$$D(s) := M_1(s)B_1(s) + M_2(s)B_2(s) + \cdots + M_v(s)B_v(s) \tag{8.33}$$

with $A_i(s)$ and $B_j(s)$ being *independent* interval polynomials. Write

$$A_i(s) := a_0^i + a_1^i s + a_2^i s^2 + a_3^i s^3 + \cdots + a_{n_i-1}^i s^{n_i-1} + a_{n_i} s^{n_i}$$
$$B_j(s) := b_0^j + b_1^j s + b_2^j s^2 + b_3^j s^3 + \cdots + b_{d_j-1}^j s^{d_j-1} + b_{d_j}^j s^{d_j} \tag{8.34}$$

where $a_k^i \in [a_k^{i-}, a_k^{i+}]$, for $k \in \underline{n_i}$ and $b_k^j \in [b_k^{j-}, b_k^{j+}]$, for $k \in \underline{d_j}$, and $L_i(s)$ and $M_j(s)$ are fixed polynomials in s. Let

$$\underline{A}(s) := [A_1(s), A_2(s), \cdots, A_u(s)], \quad \underline{B}(s) := [B_1(s), B_2(s), \cdots, B_v(s)]. \tag{8.35}$$

Let us define the sets

$$\mathbf{A}_i(s) := \{A_i(s) \ : \ a_0^i + a_1^i s + a_2^i s^2 + \cdots + a_{n_i}^i s^{n_i}, \ a_k^i \in [a_k^{i-}, a_k^{i+}], \text{ for } k \in \underline{n_i}\}$$
$$\mathbf{B}_j(s) := \{B_j(s) \ : \ b_0^j + b_1^j s + b_2^j s^2 + \cdots + b_{d_j}^j s^{d_j}, \ b_k^j \in [b_k^{j-}, b_k^{j+}], \text{ for } k \in \underline{d_j}\}$$

$$\mathbf{N}(s) := \left\{ \sum_{i=1}^{u} L_i(s)A_i(s) \ : \ (A_1(s), \cdots, A_u(s)) \in \mathbf{A}_1(s) \times \cdots \times \mathbf{A}_u(s) \right\}$$
$$\mathbf{D}(s) := \left\{ \sum_{i=1}^{v} M_i(s)B_i(s) \ : \ (B_1(s), \cdots, B_v(s)) \in \mathbf{B}_1(s) \times \cdots \times \mathbf{B}_v(s) \right\}$$

and the corresponding set of uncertain systems

$$\mathbf{G}(s) := \left\{ \frac{N(s)}{D(s)} \ : \ (N(s), D(s)) \in (\mathbf{N}(s) \mathrm{x} \mathbf{D}(s)) \right\} := \frac{\mathbf{N}(s)}{\mathbf{D}(s)} \tag{8.36}$$

is called a *linear interval system*. The Kharitonov polynomials and segments associated with $\mathbf{A}_i(s)$ are denoted $\mathcal{K}_{A_i}(s)$ and $\mathcal{S}_{A_i}(s)$, respectively. $\mathcal{K}_{B_k}(s)$ and $\mathcal{S}_{B_k}(s)$ are defined similarly. Now let us define

$$\mathbf{A}_{\mathrm{K}}(s) := \mathcal{K}_{A_1}(s) \times \cdots \times \mathcal{K}_{A_u}(s), \qquad \mathbf{B}_{\mathrm{K}}(s) := \mathcal{K}_{B_1}(s) \times \cdots \times \mathcal{K}_{B_v}(s) \tag{8.37}$$

and

$$\mathbf{A}_{\mathrm{E}}^k(s) := \mathcal{K}_{A_1}(s) \times \cdots \times \mathcal{K}_{A_{k-1}}(s) \times \mathcal{S}_{A_k}(s) \times \mathcal{K}_{A_{k+1}}(s) \cdots \times \mathcal{K}_{A_u}(s),$$
$$\mathbf{B}_{\mathrm{E}}^j(s) := \mathcal{K}_{B_1}(s) \times \cdots \times \mathcal{K}_{B_{j-1}}(s) \times \mathcal{S}_{B_j}(s) \times \mathcal{K}_{B_{j+1}}(s) \cdots \times \mathcal{K}_{B_v}(s) \tag{8.38}$$

for $k \in \underline{u}$ and $j \in \underline{v}$. Let

$$\mathbf{A}_{\mathrm{E}}(s) := \cup_{i=1}^{u} \mathbf{A}_{\mathrm{E}}^i(s), \qquad \mathbf{B}_{\mathrm{E}}(s) := \cup_{i=1}^{v} \mathbf{B}_{\mathrm{E}}^i(s). \tag{8.39}$$

Now introduce

$$\mathbf{N}_{\mathrm{K}}(s) := \left\{ N(s) \ : \ N(s) = \sum L_i(s)A_i(s), (A_1(s), \cdots, A_u(s)) \in \mathbf{A}_{\mathrm{K}}(s) \right\}$$
$$\mathbf{N}_{\mathrm{E}}(s) := \left\{ N(s) \ : \ N(s) = \sum L_i(s)A_i(s), (A_1(s), \cdots, A_u(s)) \in \mathbf{A}_{\mathrm{E}}(s) \right\} \quad (8.40)$$

Similar definitions hold for $\mathbf{D}_{\mathrm{K}}(s)$ and $\mathbf{D}_{\mathrm{E}}(s)$, and the extremal subsets are:

$$(\mathbf{N}(s)\mathrm{x}\mathbf{D}(s))_{\mathrm{E}} := (\mathbf{N}_{\mathrm{K}}(s)\mathrm{x}\mathbf{D}_{\mathrm{E}}(s)) \cup (\mathbf{N}_{\mathrm{E}}(s)\mathrm{x}\mathbf{D}_{\mathrm{K}}(s)). \quad (8.41)$$

The extremal subset of the family $\mathbf{G}(s)$ is:

$$\mathbf{G}_{\mathrm{E}}(s) := \left\{ \frac{N(s)}{D(s)} \ : \ (N(s), D(s)) \in (\mathbf{N}(s)\mathrm{x}\mathbf{D}(s))_{\mathrm{E}} \right\} := \frac{\mathbf{N}_{\mathrm{K}}(s)}{\mathbf{D}_{\mathrm{E}}(s)} \cup \frac{\mathbf{N}_{\mathrm{E}}(s)}{\mathbf{D}_{\mathrm{K}}(s)}. \quad (8.42)$$

In words the extremal set is obtained by fixing all the A_i, B_j at Kharitonov vertices except one and letting this one range over the Kharitonov segments. We remark here that in the more general case where some of the A_i and B_j happen to be identical the same procedure for constructing the extremal subset will work except that this constraint must be imposed on $\mathbf{G}_{\mathrm{E}}(s)$.

With the above definitions we can verify that $\mathbf{N}(j\omega)$ and $\mathbf{D}(j\omega)$ are polygons. The vertices of $\mathbf{N}(j\omega)$ are contained in the set $\mathbf{N}_{\mathrm{K}}(j\omega)$ and the edges of $\mathbf{N}(j\omega)$ are contained in $\mathbf{N}_{\mathrm{E}}(j\omega)$. Similar relations hold for $\mathbf{D}(j\omega)$. From this, it follows easily that for the class of linear interval systems $\mathbf{G}(s)$ defined in (8.33) - (8.36) each of the statements given in Theorems 8.1 - 8.8 remains valid with $\mathbf{G}_{\mathrm{E}}(s)$ defined as in (8.42). The conditions are constructive because here again $\mathbf{G}_{\mathrm{E}}(s)$ is a set of one parameter families. We illustrate the above calculations in the example below.

Example 8.5. Consider the linear interval system

$$G(s) = \frac{L_1(s)A_1(s)}{M_1(s)B_1(s) + M_2(s)B_2(s)} = \frac{5(\gamma_1 s + \gamma_0)}{s(\alpha_3 s^3 + \alpha_2 s^2) + (\beta_2 s^2 + \beta_1 s)}$$

where

$$\gamma_1 \in [0.40, 1.60], \quad \gamma_0 \in [19.40, 20.60], \quad \alpha_3 \in [0.40, 1.60],$$
$$\alpha_2 \in [7.40, 8.60], \quad \beta_2 \in [31.4, 32.6], \quad \beta_1 \in [74.45, 75.65].$$

Here, we illustrate the construction of Bode, Nyquist, and Nichols templates. First we write the Kharitonov polynomials of $A_1(s)$, $B_1(s)$, and $B_2(s)$:

$$K^1_{A_1}(s) = 1.6s^3 + 8.6s^2 \qquad K^2_{A_1}(s) = 0.4s^3 + 8.6s^2$$
$$K^3_{A_1}(s) = 1.6s^3 + 7.4s^2 \qquad K^4_{A_1}(s) = 0.4s^3 + 7.4s^2$$
$$K^1_{B_1}(s) = 32.6s^2 + 74.45s \qquad K^2_{B_1}(s) = 32.6s^2 + 75.65s$$
$$K^3_{B_1}(s) = 31.4s^2 + 74.45s \qquad K^4_{B_1}(s) = 31.4s^2 + 75.65s$$
$$K^1_{B_2}(s) = 0.4s + 19.4s \qquad K^2_{B_2}(s) = 1.6s^2 + 19.4s$$
$$K^3_{B_2}(s) = 0.4s^2 + 20.6s \qquad K^4_{B_1}(s) = 1.6s^2 + 20.6s$$

Then the extremal systems we will deal with are

$$\frac{L_1(s)\left(\lambda K^i_{A_1}(s)+(1-\lambda)K^k_{A_1}(s)\right)}{M_1(s)K^l_{B_1}(s)+M_2(s)K^j_{B_2}(s)},$$

$$\frac{L_1(s)K^i_{A_1}(s)}{M_1(s)\left(\lambda K^k_{B_1}(s)+(1-\lambda)K^l_{B_1}(s)\right)+M_2(s)K^j_{B_2}(s)},$$

$$\frac{L_1(s)K^i_{A_1}(s)}{M_1(s)K^j_{B_1}(s)+M_2(s)\left(\lambda K^k_{B_2}(s)+(1-\lambda)K^l_{B_2}(s)\right)},$$

for

$$i,j=1,2,3,4;\quad (k,l)\in\{(1,2),(1,3),(2,4),(3,4)\}.$$

Figures 8.21, 8.22 and 8.23 show the Nyquist, Bode and Nichols envelopes of the system respectively.

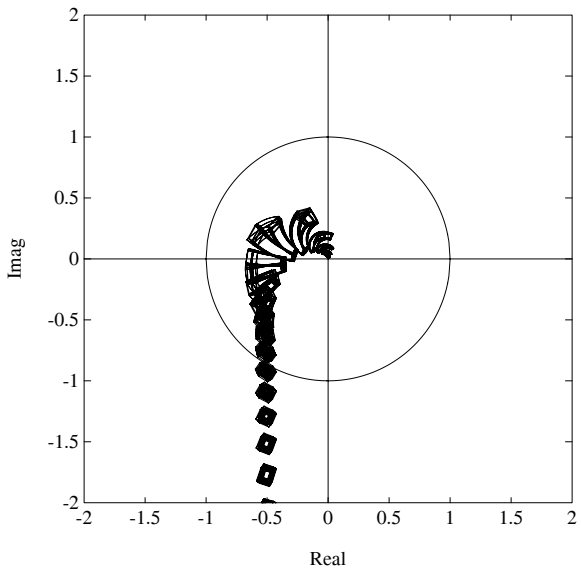

Figure 8.21. Nyquist templates of linear interval system (Example 8.5)

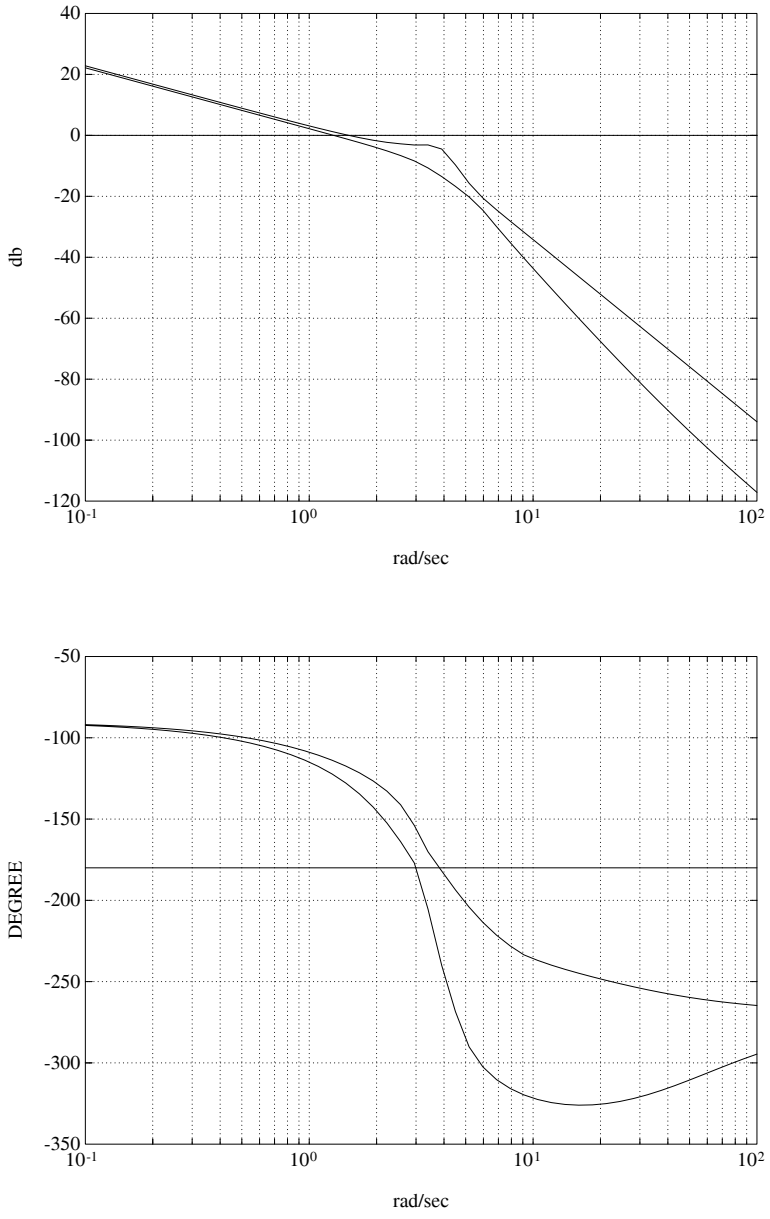

Figure 8.22. Bode envelopes of linear interval system (Example 8.5)

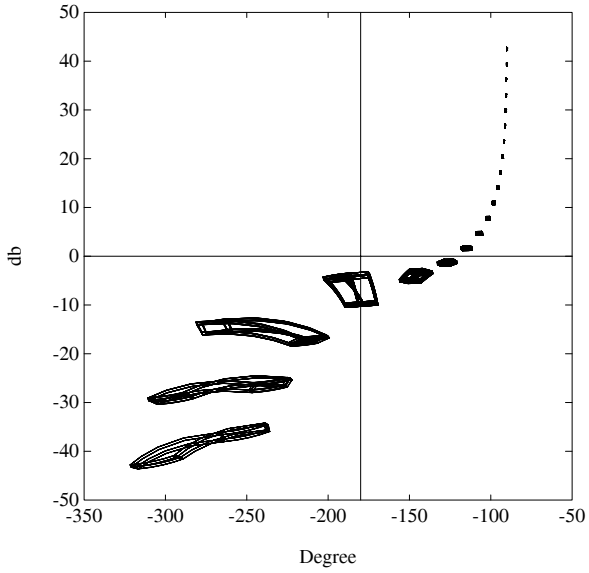

Figure 8.23. Nichols templates of linear interval system (Example 8.5)

8.7 POLYTOPIC SYSTEMS

In many models containing parametric uncertainty the only convenient representation is one where each independent parameter is explicitly displayed. In this case, we write

$$G(s) := \frac{a_1 L_1(s) + a_2 L_2(s) + \cdots + a_u L_u(s)}{b_1 M_1(s) + b_2 M_2(s) + \cdots + b_v M_v(s)} \tag{8.43}$$

and let

$$\mathbf{G}(s) := \left\{ G(s) \ : \ a_i^- \le a_i \le a_i^+, \quad b_j^- \le b_j \le b_j^+, \quad i \in \underline{u}, \quad j \in \underline{v} \right\} \tag{8.44}$$

denote the family of uncertain systems. Let

$$\mathbf{p} := [a_1, a_2, \cdots, a_u, b_1, b_2, \cdots, b_v] \tag{8.45}$$

denote the parameter vector and

$$\mathbf{\Pi} := \left\{ \mathbf{p} \ : \ a_i^- \le a_i \le a_i^+, \quad b_j^- \le b_j \le b_j^+, \quad i \in \underline{u}, \quad j \in \underline{v} \right\} \tag{8.46}$$

the uncertainty polytope. Write (8.43) as $G(s, \mathbf{p})$ to emphasize its dependence on $\mathbf{p}$. For convenience we refer to the family of systems $G(s, \mathbf{p}) : \mathbf{p} \in \mathbf{\Pi}$ represented in the form (8.43) as a *polytopic system*. Of course a polytopic system is just a special case of a linear interval system with the uncertain polynomials being of degree zero.

Let $\mathbf{\Pi}_{\mathrm{E}}$ denote the exposed edges of $\mathbf{\Pi}$ and introduce the extremal systems

$$\mathbf{G}_{\mathrm{E}}(s) := \{G(s,\mathbf{p}) \ : \ \mathbf{p} \in \mathbf{\Pi}_{\mathrm{E}}\}. \tag{8.47}$$

Now suppose that s^* is an arbitrary point in the complex plane, where the image set $\mathbf{G}(s^*)$ needs to be found. In the Hurwitz case we might have $s^* = j\omega$ and in a discrete time control system, for example, s^* could be a point on the unit circle. We have the following result.

Theorem 8.9

$$\partial\mathbf{G}(s^*) \subset \mathbf{G}_{\mathrm{E}}(s^*).$$

Proof. The proof follows from Lemma 8.1 applied to the polygons

$$Q_1 = \left\{a_1 L_1(s^*) + \cdots + a_u L_u(s^*) \ : \ a_i^- \le a_i \le a_i^+, \quad i \in \underline{u}\right\}$$
$$Q_2 = \left\{b_1 M_1(s^*) + \cdots + b_v M_v(s^*) \ : \ b_j^- \le b_j \le b_j^+, \quad j \in \underline{v}\right\}.$$

♣

All the results of Theorems 8.1 to 8.8 carry over to this general case with the extremal set $\mathbf{G}_{\mathrm{E}}(s)$ being defined by (8.47). The more general case where some $a_i,\ b_j$ are identical can be handled by imposing the same constraint on $\mathbf{G}_{\mathrm{E}}(s)$.

8.8 LINEAR FRACTIONAL TRANSFORMATIONS OF INTERVAL SYSTEMS

We have thus far assumed that our uncertain system is described by an interval system, a linear interval system, or a polytopic system model. In each of these cases we developed extremal and boundary results under the assumption that the numerator and denominator parameter sets are *disjoint* or that they perturb *independently*. On the other hand, we saw that these extremal and boundary results carry over to all the feedback system transfer functions even though, in some of these, the numerator and denominator do contain *common* uncertain parameters. A natural question to ask therefore is: What is a useful general model with interval parametric uncertainty, incorporating dependencies between numerator and denominator parameters, for which boundary or extremal results can be obtained? It turns out that a very broad class of systems of this type can be encompassed under the class of *linear fractional transformations* of an linear interval system.

Therefore, let us suppose that $\mathbf{G}(s)$ is a linear interval system (see (8.36)) with independent uncertain interval polynomials $A_i(s), B_j(s)$ and let $\mathbf{G}_{\mathrm{E}}(s)$ denote the extremal subset as defined in Section 8.6. Let $P(s), Q(s), R(s), S(s)$ be four arbitrary fixed functions and consider the transformation

$$H(s) = \frac{P(s)G(s) + Q(s)}{R(s)G(s) + S(s)}.$$

We suppose that the transformation is well defined ($R(s)G(s) + S(s) \neq 0$) and refer to such a transformation as a *linear fractional transformation*. Obviously $H(s)$ contains, in general, common interval parameters in the numerator and denominator even though $G(s)$ has only independent parameters in the numerator and denominator. As before let

$$\mathbf{H}(s) := \left\{ \frac{P(s)G(s) + Q(s)}{R(s)G(s) + S(s)} : G(s) \in \mathbf{G}(s) \right\}$$

and let

$$\mathbf{H}_{\mathrm{E}}(s) := \left\{ \frac{P(s)G(s) + Q(s)}{R(s)G(s) + S(s)} : G(s) \in \mathbf{G}_{\mathrm{E}}(s) \right\}.$$

We show below that under mild conditions on the set $P(s), Q(s), R(s), S(s)$ the boundary of the set $\mathbf{H}(j\omega)$ is generated by the extremal set $\mathbf{G}_{\mathrm{E}}(j\omega)$.

Theorem 8.10 *If*

$$P(j\omega)S(j\omega) - Q(j\omega)R(j\omega) \neq 0$$

we have

$$\partial\mathbf{H}(j\omega) \subset \mathbf{H}_{\mathrm{E}}(j\omega).$$

Proof. We know that the boundary of $\mathbf{G}(j\omega)$ is contained in $\mathbf{G}_{\mathrm{E}}(j\omega)$. Therefore all we need to show is that the transformation $G(s) \longrightarrow H(s)$ is a boundary preserving mapping. Write

$$P(j\omega) = p, \quad Q(j\omega) = q, \quad R(j\omega) = r, \quad S(j\omega) = s, \quad G(j\omega) = g, \quad H(j\omega) = h.$$

We see that under the assumption stated ($ps - qr \neq 0$), we can write

$$h = \left[\frac{qr - ps}{r}\right]\left[\frac{1}{rg + s}\right] + \frac{p}{r} = \frac{pg + q}{rg + s}.$$

Thus h is obtained from g by a sequence of operations consisting of multiplication by a complex number, addition of a complex number and inversion of a complex number. Each of these are boundary preserving operations (see Lemma 8.1) and so the result follows. ♣

Remark 8.3. With this result in hand it is easy to see that all the extremal and boundary results stated in this chapter carry over to linear fractional transformations of linear interval systems. The practical implication of this result is that by adjusting the set $P(s), Q(s), R(s), S(s)$ we can account for a large class of interdependencies between the perturbations. It is easy to show that all the transfer functions that occur in a closed loop system can be shown to be linear fractional transformations of $G(s)$ which satisfy the restriction stated in the theorem above. Thus it is not surprising that the extremal results stated in Theorem 8.3 hold. Finally, we point out that the boundary generating property of $\mathbf{G}_{\mathrm{E}}(s)$ continues to hold for any further linear fractional transformations applied to $H(s)$.

Example 8.6. Let us consider the block diagram shown in Figure 8.24. The closed

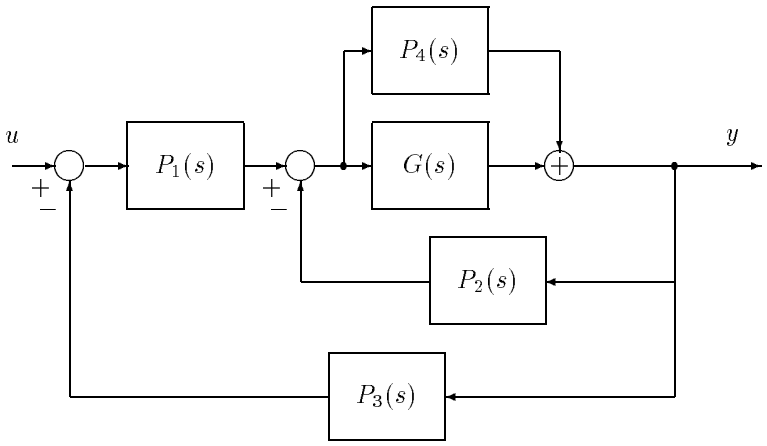

Figure 8.24. A feedback system

loop transfer function of the system is

$$\begin{aligned}\frac{y(s)}{u(s)} &= \frac{P_1(s)P_4(s) + P_1(s)G(s)}{1 + [P_1(s)P_3(s) + P_2(s)]\,P_4(s) + [P_1(s)P_3(s) + P_2(s)]\,G(s)} \\ &= H(s).\end{aligned}$$

If $G(s)$ belongs to an interval transfer function family $\mathbf{G}(s)$, then the family of output transfer functions is

$$\mathbf{H}(s)$$

$$= \left\{ \frac{P_1(s)P_4(s) + P_1(s)G(s)}{1 + [P_1(s)P_3(s) + P_2(s)]\,P_4(s) + [P_1(s)P_3(s) + P_2(s)]\,G(s)} : G(s) \in \mathbf{G}(s) \right\}$$

$$= \left\{ \frac{\overbrace{P_1(s)}^{P(s)}\,G(s) + \overbrace{P_1(s)P_4(s)}^{Q(s)}}{\underbrace{[P_1(s)P_3(s) + P_2(s)]}_{R(s)}\,G(s) + \underbrace{1 + [P_1(s)P_3(s) + P_2(s)]\,P_4(s)}_{S(s)}} : G(s) \in \mathbf{G}(s) \right\}.$$

Thus, if

$$P(j\omega)S(j\omega) - Q(j\omega)R(j\omega) \neq 0,$$

we have

$$\partial\mathbf{H}(j\omega) \subset \mathbf{H}_{\mathrm{E}}(j\omega).$$

The point is, that even though $\mathbf{H}(s)$ is *not* an interval transfer function, the boundary of $\mathbf{H}(j\omega)$ is captured by replacing $\mathbf{G}(s)$ by the elements of the extremal set

$\mathbf{G}_E(s)$ which is a considerable saving. Similar results hold for the Nyquist and Bode envelopes, and in fact all extremal properties of $\mathbf{H}(s)$ will occur on the subset $\mathbf{H}_E(s)$.

8.9 ROBUST PARAMETRIC CLASSICAL DESIGN

We illustrate the utility of the above tools in extending the design techniques of classical control to systems containing parameter uncertainty. The requirement of robust design is that the design specifications must be satisfied over the entire parameter set. Thus the worst case values must be acceptable. Since these worst case values occur over the extremal set $\mathbf{G}_{\mathrm{E}}(s)$, it suffices to verify that the specifications are met over this set.

8.9.1 Guaranteed Classical Design

Example 8.7. Consider the interval plant

$$\mathbf{G}(s) = \frac{n_0}{d_3 s^3 + d_2 s^2 + d_1 s + d_0}$$

with $n_0 \in [10, 20]$, $d_3 \in [0.06, 0.09]$, $d_2 \in [0.2, 0.8]$, $d_1 \in [0.5, 1.5]$, $d_0 = 0$. The objective is to design a controller so that the closed loop system

a) is robustly stable under all parameter perturbations,

b) possesses a guaranteed phase margin of at least 45°. In other words the worst case phase margin over the set of uncertain parameters must be better than 45°, and

c) possesses a bandwidth greater than or equal to 0.1 [rad/sec] with a reasonable value of resonant peak M_p.

We simply follow the standard classical control design techniques with the new tools developed here. First we construct the Bode envelopes of the open loop interval plant $\mathbf{G}(s)$. From the magnitude and phase envelopes, we observe that the worst case phase margin of 50° is achieved if the gain crossover frequency ω_c' is at 0.5 [rad/sec]. In order to bring the magnitude envelope down to 0 [dB] at the new crossover frequency ω_c', the phase lag compensator of the form

$$C(s) = \frac{1 + aTs}{1 + Ts}, \qquad a < 1$$

must provide the amount of attenuation equal to the minimum value of the magnitude envelope at ω_c':

$$\max_{G(j\omega_c') \in \mathbf{G}(j\omega_c')} |G(j\omega_c')| = -20 \log_{10} a[dB].$$

Thus, we have $a = 0.01$. Now we choose the corner frequency $\frac{1}{aT}$ to be one decade below ω_c':

$$\frac{1}{aT} = \left.\frac{\omega_c'}{10}\right|_{\omega_c'=0.5}$$

and we have $T = 2000$. Finally, the resulting phase lag compensator becomes

$$C(s) = \frac{1+20s}{1+2000s}.$$

Here we give some analysis to check whether the controller $C(s)$ satisfies the given design requirements. The robust stability of the closed loop system with the controller $C(s)$ may be easily determined by applying Theorem 8.1. Moreover by GKT since we use a first order controller it is only necessary to check the stability of the following vertex polynomials:

$$(1+2000s)K_d^i(s) + (1+20s)K_n^j(s), \qquad i = 1,2,3,4; j = 1,2$$

where

$$\begin{aligned} K_n^1(s) &:= 10 & K_n^2(s) &:= 20 \\ K_d^1(s) &:= 0.5s + 0.8s^2 + 0.09s^3 & K_d^2(s) &:= 1.5s + 0.8s^2 + 0.06s^3 \\ K_d^3(s) &:= 0.5s + 0.2s^2 + 0.09s^3 & K_d^4(s) &:= 1.5s + 0.2s^2 + 0.06s^3. \end{aligned}$$

The eight polynomials above are stable and this shows that the closed loop system remains stable under all parameter perturbations within the given ranges. Figure 8.25 shows the frequency response (Bode envelopes) of $\mathbf{G}(s)$ (uncompensated system) and $C(s)\mathbf{G}(s)$ (compensated system). Clearly, the guaranteed phase margin requirement of 45° is satisfied. The guaranteed gain margin of the system is 12 db. The closed loop response $|\mathbf{M}(j\omega)|$ called $\mathbf{T}^y(j\omega)$ in (8.22) is shown in Figure 8.26 where

$$\mathbf{M}(j\omega) := \mathbf{M}(s)|_{s=j\omega} := \left\{ M(s) \ : \ \frac{C(s)G(s)}{1+C(s)G(s)}, \ \ G(s) \in \mathbf{G}(s) \right\}. \tag{8.48}$$

Note that the $|\mathbf{M}(j\omega)|$ envelope shown in this figure is calculated from the result of Theorem 8.4. Figure 8.26 shows that the M_p of every system in the family lies between 1.08 and 1.3886. This also shows that the bandwidth of every system in the family lies in between 0.12 and 0.67 [rad/sec]. Thus, the design objective is achieved. Figure 8.27 shows the Nyquist plot of $C(s)\mathbf{G}(s)$. The center of the M-circle in Figure 8.27 is

$$\begin{aligned} \left(\frac{M_p^2}{1-M_p^2}, 0 \right) &= \left(\frac{1.3886^2}{1-1.3886^2}, 0 \right) \\ &= (-2.0772, 0) \end{aligned}$$

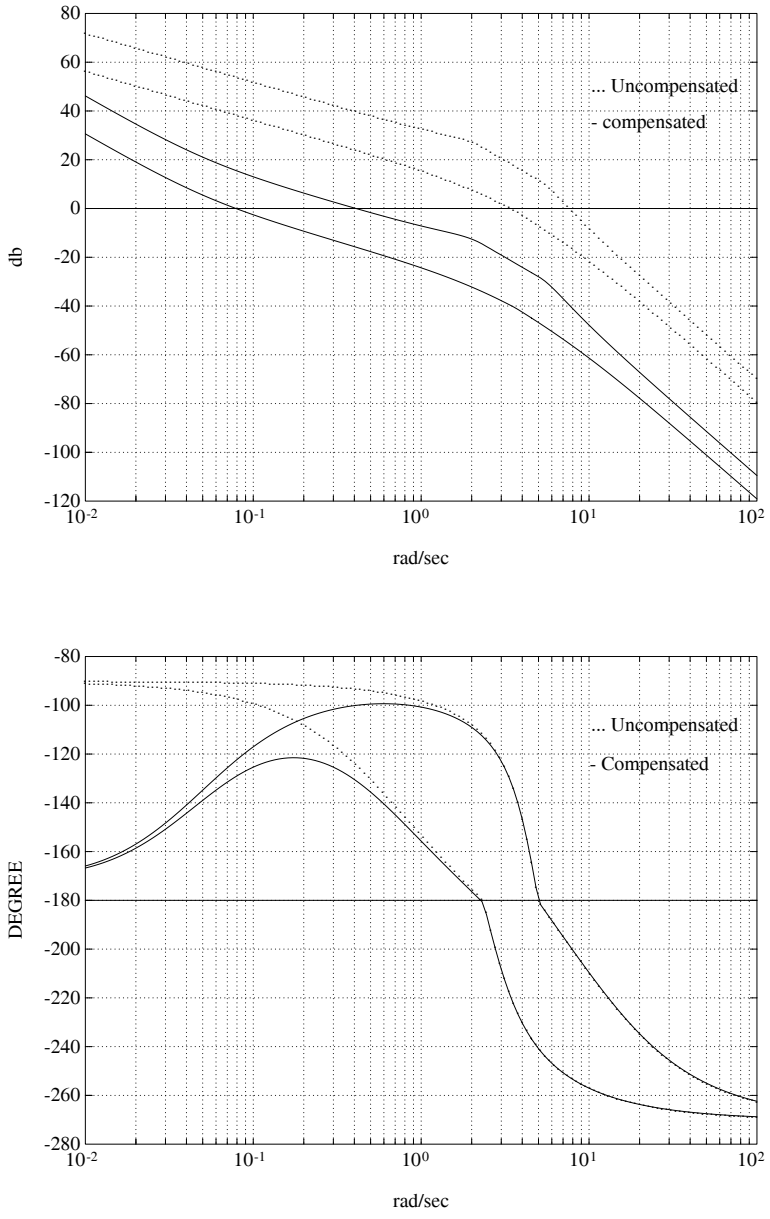

Figure 8.25. Bode envelopes of $\mathbf{G}(s)$ and $C(s)\mathbf{G}(s)$ (Example 8.7)

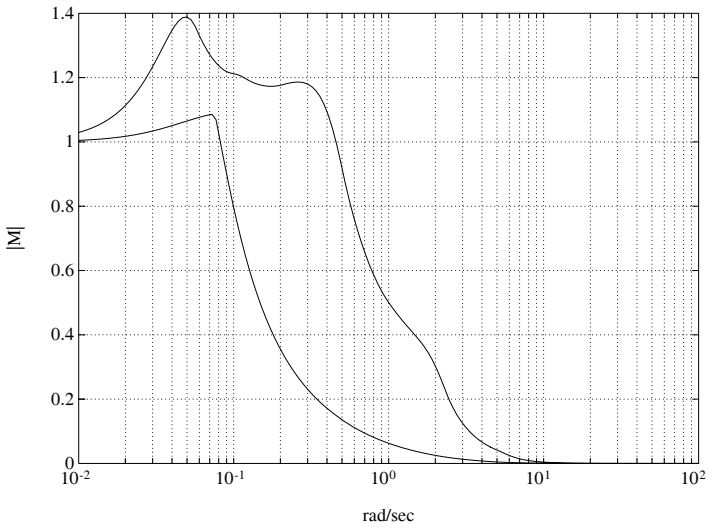

Figure 8.26. Closed-loop frequency response (Example 8.7)

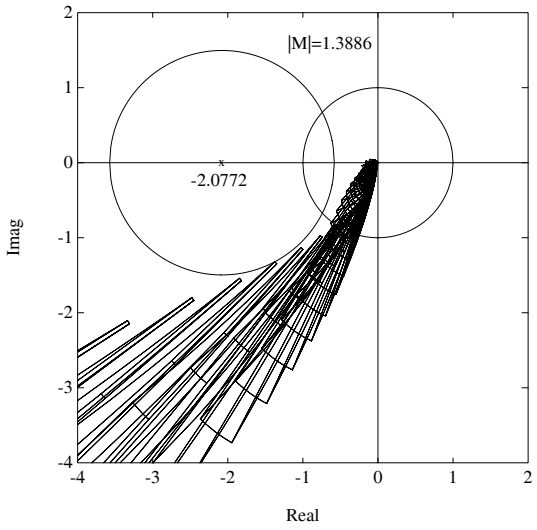

Figure 8.27. Nyquist envelope of $C(s)\mathbf{G}(s)$ with M-circle (Example 8.7)

and the radius of the circle is

$$r = \left| \frac{M_p}{1 - M_p^2} \right| = 1.496.$$

Example 8.8. (Lead-lag Compensation) We give an example of lead-lag compensation design utilizing the developments described above. Let us consider the interval plant

$$G(s) = \frac{a_0}{b_3 s^3 + b_2 s^2 + b_1 s + b_0}$$

with coefficients bounded as follows:

$$a_0 \in [5, 7], \quad b_3 \in [.09, .11], \quad b_2 \in [.9, 1.2], \quad b_1 \in [.8, 1.5], \quad b_0 \in [.1, .3]$$

The objective of the design is to guarantee that the entire family of systems has a phase margin of at least 60° and a gain margin of at least 30dB. From Figure 8.29, we observe that the phase margin 70° which is equal to the desired phase margin of 60° plus some safety factor can be obtained if the new gain-crossover frequency ω_c' is at 0.35 [rad/sec]. This means that the phase-lag compensator must reduce the maximum magnitude of $\mathbf{G}(j\omega_c')$ over the interval family to 0 [db]. Thus, we solve

$$-20 \log_{10} a = \max_{G(j\omega_c') \in \mathbf{G}(j\omega_c')} |G(j\omega_c')| = 28[\text{db}]$$

and we have

$$a = 0.0398.$$

In order that the phase lag of the compensator does not affect the phase at the new gain-crossover frequency ω_c', we choose the value of $1/aT$ to be at one decade below ω_c'. Thus,

$$T = \frac{10}{a\omega_c'} = \frac{10}{(0.0398)(0.35)} = 717.875.$$

Therefore, the lag compensator obtained is

$$C_1(s) = \frac{1 + aTs}{1 + Ts} = \frac{28.5714s + 1}{717.875s + 1}.$$

We have now achieved approximately 70° of guaranteed phase margin and 25dB of guaranteed gain margin.

To achieve the desired gain margin, we now wish to move the phase-crossover frequency ω_c'' to 4.7 [rad/sec]. If the magnitude plot does not move, we can achieve the gain margin of 35db at this frequency. Thus, we solve

$$-10 \log_{10} a = -(35 - 25) = -10[\text{db}]$$

and we have

$$a = 10.$$

Then,

$$\frac{1}{T} = \sqrt{a}\omega_c'' = \sqrt{10}(4.7) = 14.86$$

and $T = 0.0673$. Therefore, the cascaded lead compensator is

$$\begin{aligned} C_2(s) &= \frac{1}{a}\frac{1+aTs}{1+Ts} \\ &= \frac{1}{10}\frac{(10)(0.0673)s+1}{0.0673s+1} = \frac{s+1.485}{s+14.859}. \end{aligned}$$

From Figure 8.29, we verify that the compensated system provides approximately 105° of guaranteed phase margin and 50dB of guaranteed gain margin. Therefore, the controller

$$C(s) = C_2(s)C_1(s) = \frac{s+1.5}{s+15}\frac{28.5714s+1}{717.682s+1}$$

attains the design specifications robustly. Figures 8.28, 8.29 and 8.30 show the Nyquist, Bode and Nichols envelopes of the uncompensated and compensated systems.

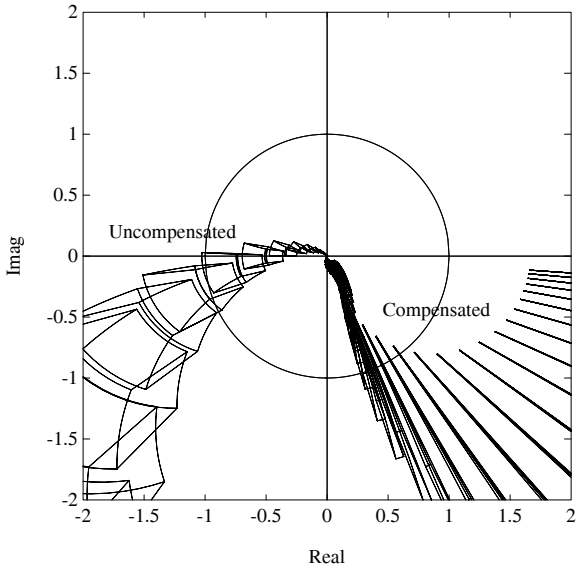

Figure 8.28. Nyquist envelope (Example 8.8)

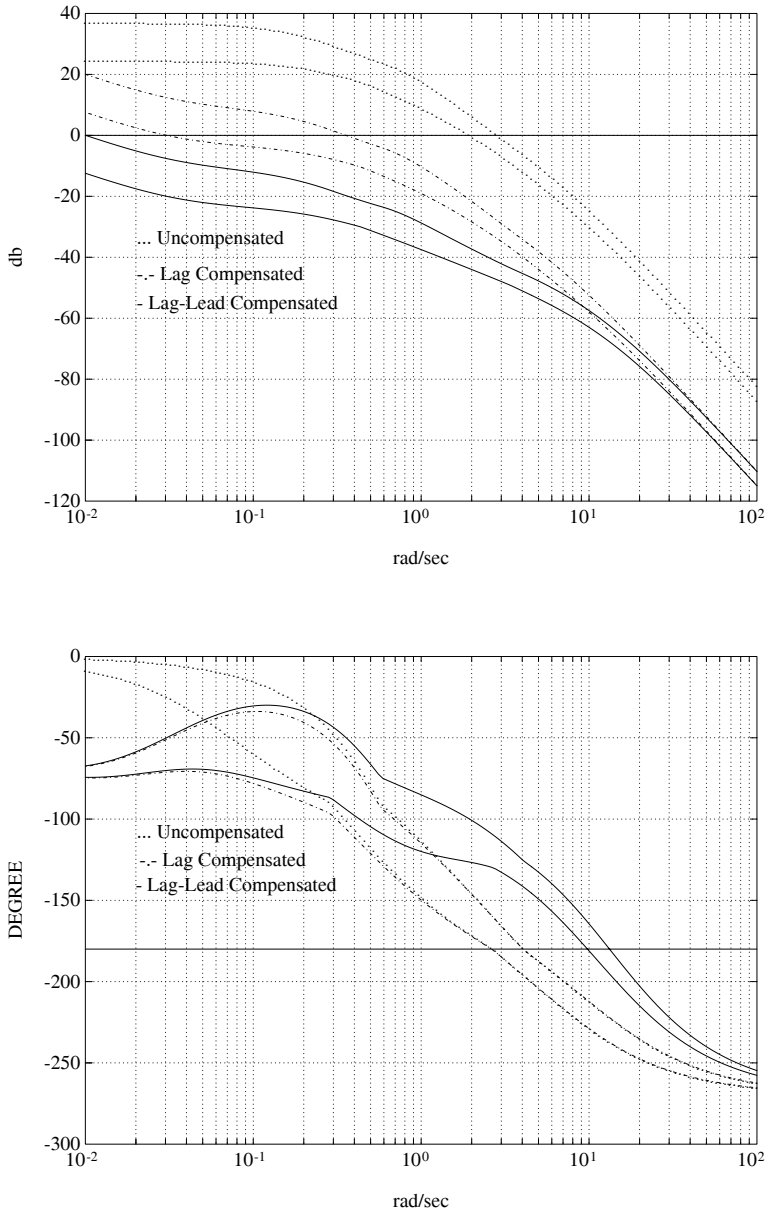

Figure 8.29. Bode envelopes (Example 8.8)

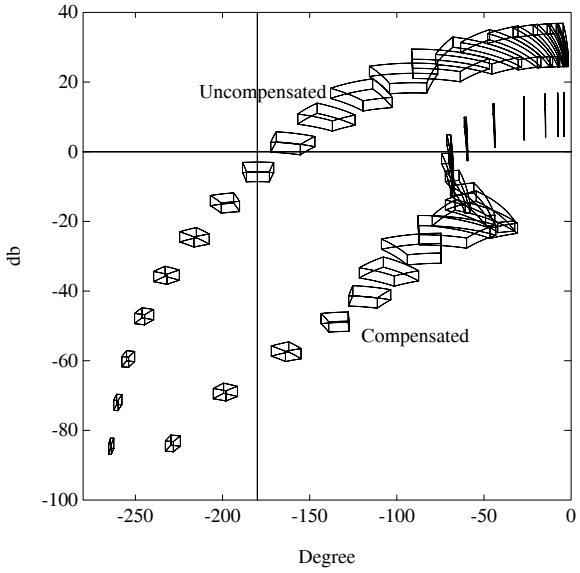

Figure 8.30. Nichols templates (Example 8.8)

Example 8.9. (PI Compensation) Consider the plant

$$G(s) = \frac{n_1 s + 1}{.02s^4 + d_3 s^3 + d_2 s^2 + .04s}$$

with its coefficients bounded by given intervals as follows:

$$n_1 \in [.35, .45], \quad d_3 \in [.25, .35], \quad b_2 \in [.9, 1.1]$$

The objective of the design is to guarantee that the entire family of closed loop systems has a phase margin of at least 45°.

Here we design a PI compensator of the form

$$C(s) = K_P + \frac{K_I}{s}.$$

From Figure 8.32 we see that the new gain-crossover frequency ω_c' should be moved to 0.034 [rad/sec]. Since the maximum magnitude at ω_c' is 55 [db], we let

$$G_p(j\omega_c') := \max_{G(j\omega_c') \in \mathbf{G}(j\omega_c')} |G(j\omega_c')| = -20 \log_{10} K_p = 54.89[\text{db}]$$

from which

$$K_P = 10^{-|G_p(j\omega_c')|[\text{db}]/20} = 10^{-54.89/20} = 0.0018.$$

In order that the phase lag of the PI compensator not effect the phase of the compensated system at ω_c', we choose the corner frequency K_I/K_P to be one decade below ω_c'. Thus,

$$K_I = \frac{\omega_c'}{10} K_P = \frac{0.034}{10}(0.0018) = 6.12 \times 10^{-6}.$$

Therefore, the PI compensator obtained is

$$C(s) = \frac{6.12 \times 10^{-6} + .0018s}{s}.$$

Figure 8.31 shows the Nyquist envelope while Figures 8.32 and 8.33 show the Bode and Nichols envelopes of the uncompensated and compensated systems. We can see that the phase margin specifications are robustly achieved.

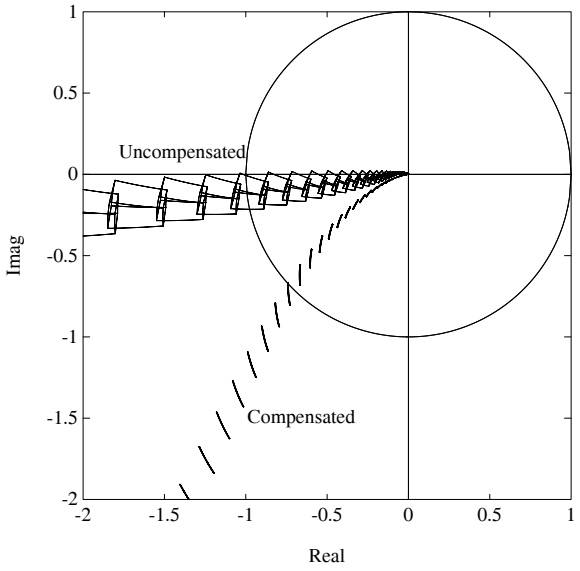

Figure 8.31. Nyquist envelope (Example 8.9)

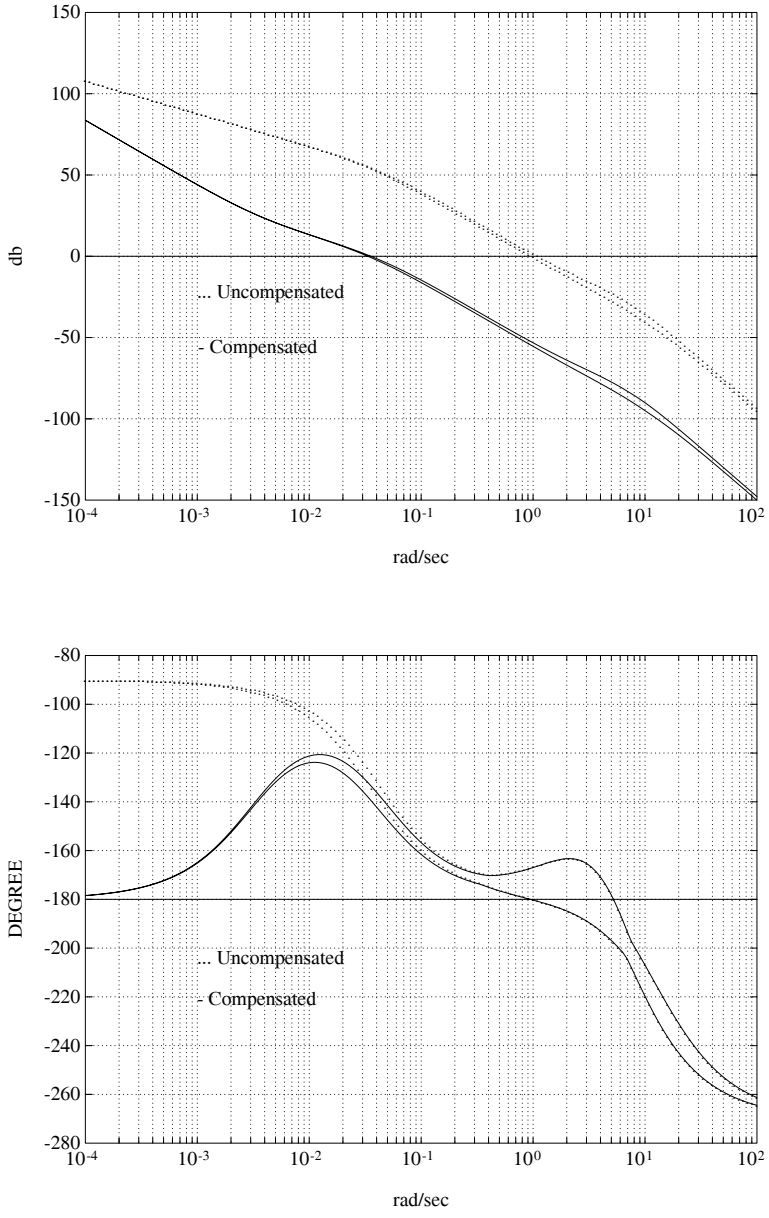

Figure 8.32. Bode envelopes (Example 8.9)

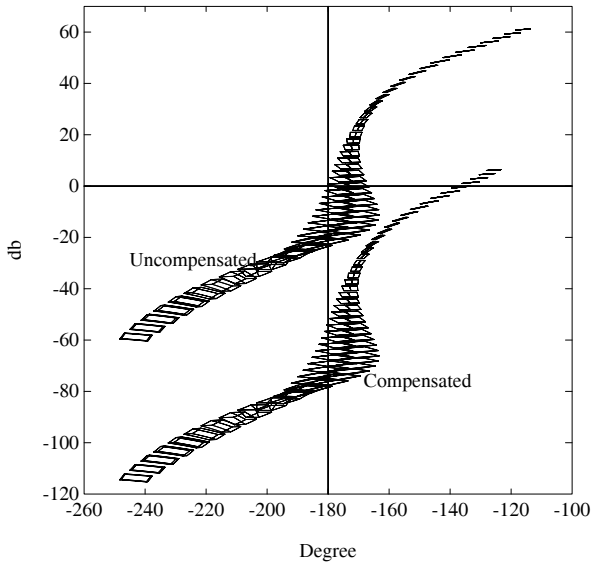

Figure 8.33. Nichols templates (Example 8.9)

8.9.2 Optimal Controller Parameter Selection

In the design problem, we interchange the role of plant and controller, and consider a family of controllers stabilizing a fixed plant $G(s)$. The design problem here is to select from the controller family the *best* parameter value according to some criterion. This type of problem is common in practice. Let us consider for example that this parameter selection is to be made to maximize gain margin or phase margin. The set of controller parameters may be given in terms of bounded values. In other words, we have a interval family of controllers stabilizing a fixed plant. To maximize the gain margin (or phase margin) over this set, we explore the boundary results given earlier.

In Section 8.4 we showed that the minimum gain margin (or phase margin) occurs over the extremal set. In practice, the maximum gain margin (or phase margin) will also frequently occur over the same set. To see this, we argue as follows. The Nyquist boundary of the system cuts the real axis over the range A to B (see Figure 8.34 and Figure 8.35). The point A corresponds to the minimum gain margin of the family. The point B is a potential candidate for the maximum gain margin (gain margin = $1/OB$). Corresponding to the point B, there exists a set C_B of admissible (parameters lie within the given intervals) controllers whose Nyquist plots pass through the point B. Suppose that one of these controllers is such that the Nyquist plot does *not* cut the real axis at any other point (see Figure

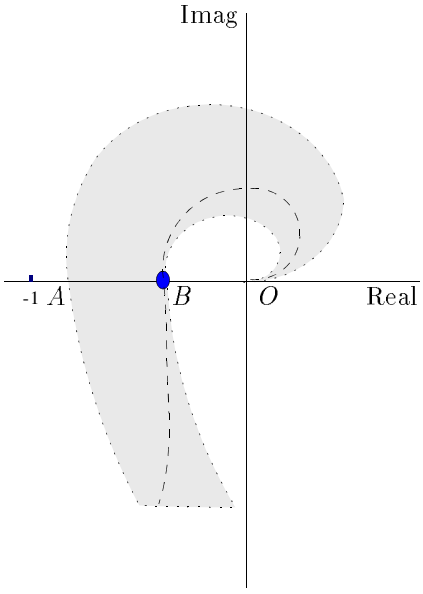

Figure 8.34. A system that delivers the maximum gain margin

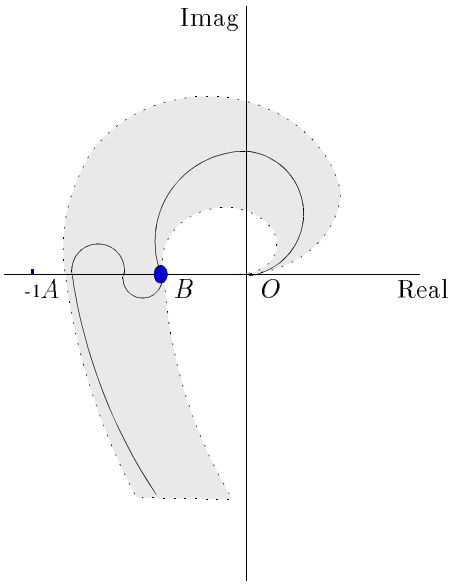

Figure 8.35. A system that does not deliver the maximum gain margin

8.34). It is clear that this controller delivers the maximum gain margin $(1/OB)$ and is the optimally robust gain margin controller in the family. We can see that the maximum gain margin will be unrealizable only if each and every controller in C_B happens to cut the real axis at another point also (see Figure 8.35). Based on the above arguments, we suggest the following design procedure. First, check whether the given family of interval controllers stabilizes the plant $G(s)$ by using the GKT (Chapter 7). If so, we use this set of controllers. Otherwise, we determine the parametric stability margin around the nominal values of controller parameters and create the largest interval stabilizing controller family around this nominal. From this controller set we can find the controller parameters that provide the maximum gain or phase margin. This can be done by generating the Nyquist envelope of the family using the development discussed earlier. If the margin obtained is not satisfactory, we reset the controller parameters to the new nominal corresponding to the point B and create a new interval stabilizing family. We repeat this procedure until a satisfactory margin is achieved or the improvement of the margin is negligibly small. The set of stabilizing interval controllers can be determined by many different methods; for example the locus introduced by Tsypkin and Polyak (Chapter 4) may be used. Of course, there is no guarantee that a globally optimum design will be achieved by this method. However, a satisfactory robust design will often result.

Example 8.10. Consider the feedback system with the plant transfer function

$$G(s) := \frac{250}{.025s^2 + 1.75s + 30}$$

and controller transfer function

$$C(s) := \frac{\alpha s + 1}{s^2 + \beta s + \gamma}.$$

The nominal values of controller parameters are

$$\alpha_0 = 5, \quad \beta_0 = 2, \quad \gamma_0 = 1.$$

The phase margin of the given system with the nominal values of controller parameters is 19.55°. The objective is to tune the three controller parameters so that the resulting system has a phase margin of approximately 45°. We first find the ℓ_2 parametric stability margin r_1 around the nominal values of parameters $(\alpha_0, \beta_0, \gamma_0)$ by using the method proposed by Tsypkin and Polyak (Chapter 4). From this value of r_1, which was obtained as $r_1 = 1$, we create the family of stabilizing controllers in the form of an interval transfer function $\mathbf{C}_1(s)$. Using this interval controller family, we create the corresponding Nyquist envelope which shows the maximum obtainable phase margin of 29.85°. Using the formulas developed previously, we select the parameter values $(\alpha_1, \beta_1, \gamma_1)$, and consequently the controller $C(s, \alpha_1, \beta_1, \gamma_1) \in \mathbf{C}_1(s)$ that produces the maximum phase margin of 29.85°. Since the resulting controller $C(s, \alpha_1, \beta_1, \gamma_1)$ does not satisfy the given requirement, we proceed with a second

iteration. The parametric stability margin around $(\alpha_1, \beta_1, \gamma_1)$ we found is again 1. We now create a new interval family $\mathbf{C}_2(s)$ of stabilizing controllers. Using the same procedure as before, we find the controller $C_2(s, \alpha_2, \beta_2, \gamma_2) \in \mathbf{C}_2(s)$. This produces the maximum phase margin of 43.76°. In the table below we present the successive designs through several iterations and Figure 8.36 shows the Nyquist plot of the optimal system for each iteration.

iteration i	parameter ranges (α, β, γ)	parameter selected $(\alpha_i, \beta_i, \gamma_i)$	phase margin
0	–	$(5, 2, 1)$	19.55°
1	$([4, 6], [1, 3], [0, 2])$	$(4, 3, 2)$	29.85°
2	$([3, 5], [2, 4], [1, 3])$	$(3, 4, 1)$	43.76°

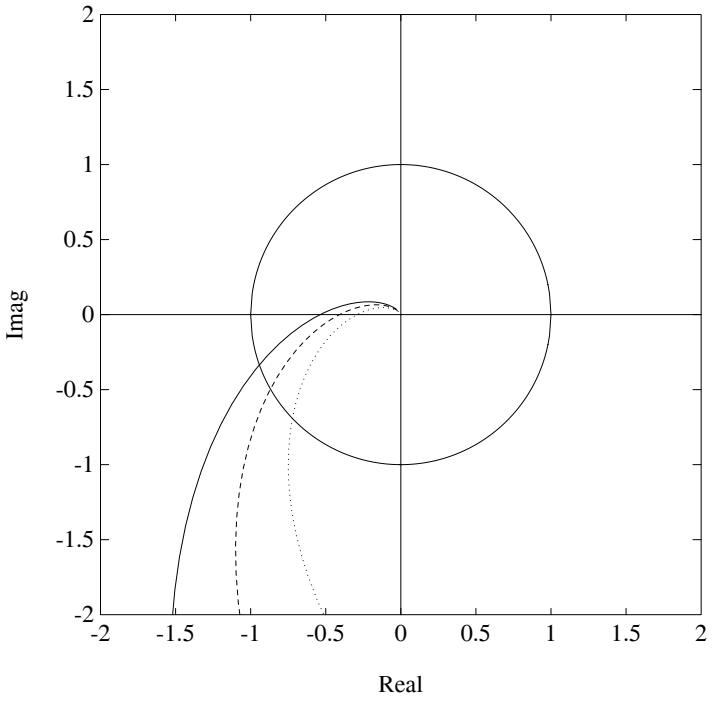

Figure 8.36. Nyquist plots of optimal systems (Example 8.10)

8.9.3 Discrete Time Control Systems

The frequency templates of discrete interval control systems can also be constructed similarly. We still use the basic geometric facts regarding the addition, multipli-

cation and division of complex plane image sets discussed here; however, the main simplifying tool used in the case of continuous systems, the GKT, is no longer applicable here. We illustrate this by an example.

Example 8.11. Consider the discrete-time feedback system shown in Figure 8.37. Let the interval plant $\mathbf{G}(z)$ and the controller $C(z)$ be

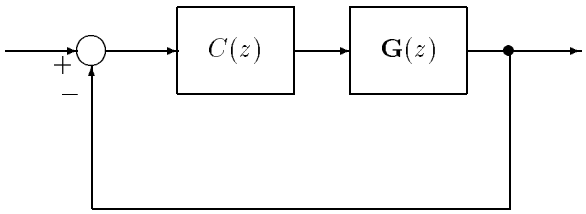

Figure 8.37. A discrete time feedback system (Example 8.11)

$$\mathbf{G}(z) = \frac{z+\alpha}{z^2+\beta z+\gamma} \quad \text{and} \quad C(z) = \frac{-0.2z-0.35}{z+3}$$

where

$$\alpha \in [0.8, 1.2] := [\alpha^-, \alpha^+],\ \beta \in [1.8, 2.2] := [\beta^-, \beta^+],\ \gamma \in [2.8, 3.2] := [\gamma^-, \gamma^+].$$

Then we have the extremal subset $\mathbf{G}_{\mathrm{E}}(z)$ consisting of the following 12 systems:

$$G_{\mathrm{E}_1}(z) = \frac{z+(\lambda\alpha^- + (1-\lambda)\alpha^+)}{z^2+\beta^- z+\gamma^-}, \qquad G_{\mathrm{E}_2}(z) = \frac{z+(\lambda\alpha^- + (1-\lambda)\alpha^+)}{z^2+\beta^+ z+\gamma^-}$$

$$G_{\mathrm{E}_3}(z) = \frac{z+(\lambda\alpha^- + (1-\lambda)\alpha^+)}{z^2+\beta^- z+\gamma^+}, \qquad G_{\mathrm{E}_4}(z) = \frac{z+(\lambda\alpha^- + (1-\lambda)\alpha^+)}{z^2+\beta^+ z+\gamma^+}$$

$$G_{\mathrm{E}_5}(z) = \frac{z+\alpha^-}{z^2+(\lambda\beta^- + (1-\lambda)\beta^+)z+\gamma^-}$$

$$G_{\mathrm{E}_6}(z) = \frac{z+\alpha^-}{z^2+(\lambda\beta^- + (1-\lambda)\beta^+)z+\gamma^+}$$

$$G_{\mathrm{E}_7}(z) = \frac{z+\alpha^+}{z^2+(\lambda\beta^- + (1-\lambda)\beta^+)z+\gamma^-}$$

$$G_{\mathrm{E}_8}(z) = \frac{z+\alpha^+}{z^2+(\lambda\beta^- + (1-\lambda)\beta^+)z+\gamma^+}$$

$$G_{\mathrm{E}_9}(z) = \frac{z + \alpha^-}{z^2 + \beta^- z + (\lambda\gamma^- + (1-\lambda)\gamma^+)}$$
$$G_{\mathrm{E}_{10}}(z) = \frac{z + \alpha^-}{z^2 + \beta^+ z + (\lambda\gamma^- + (1-\lambda)\gamma^+)}$$
$$G_{\mathrm{E}_{11}}(z) = \frac{z + \alpha^+}{z^2 + \beta^- z + (\lambda\gamma^- + (1-\lambda)\gamma^+)}$$
$$G_{\mathrm{E}_{12}}(z) = \frac{z + \alpha^+}{z^2 + \beta^+ z + (\lambda\gamma^- + (1-\lambda)\gamma^+)}$$

where in each case λ ranges over $[0, 1]$.

By searching over the family $\mathbf{G}_{\mathrm{E}}(z)$ with $z = e^{j\omega T}$ for $\omega \in [0, \infty)$ and a fixed T, we can obtain the frequency templates of the system. For illustration, the Bode envelopes of the above discrete time feedback system are given in Figure 8.38 for $T = 1$. The Nyquist and Nichols envelopes can also be generated similarly.

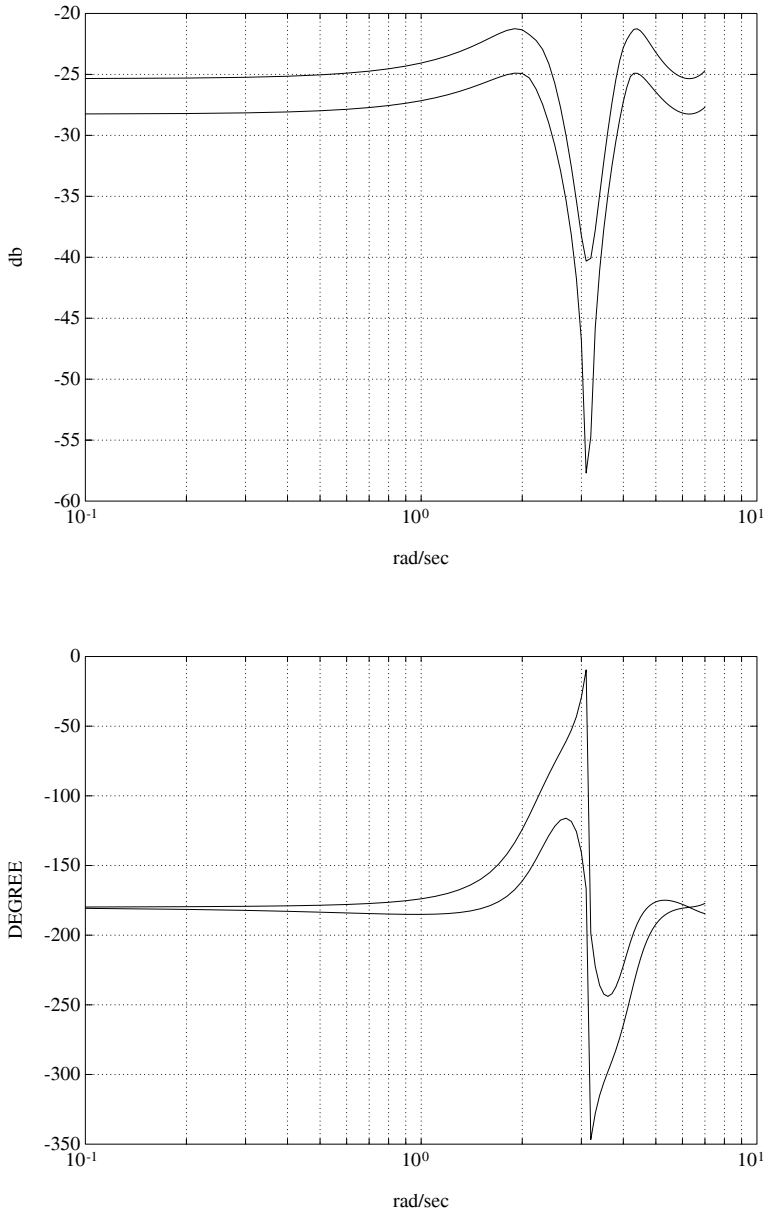

Figure 8.38. Bode envelopes (Example 8.11)

8.10 EXERCISES

8.1 Consider the family of transfer functions

$$\mathbf{G}(s) = \frac{4s^3 + \alpha_2 s^2 + \alpha_1 s + 5}{s^4 + 10\beta_3 s^3 + \beta_2 s^2 + (\beta_1 + 2\gamma_1)s}$$

where $\alpha_2, \in [1, 2], \alpha_1 \in [-2, 3]$, $\beta_3 \in [-1, 1]$, $\beta_2 \in [0.5, 1.5]$, $\beta_1 \in [-0.5, 1]$, $\gamma_1 \in [-4, -1]$. Determine a) the frequency template $\mathbf{G}(j\omega)$ at $\omega = 1, 10, 100$, b) the Nyquist, Bode and Nichols templates of $\mathbf{G}(s)$.

8.2 Consider the interval system

$$\mathbf{G}(s) = \frac{\mathbf{N}(s)}{\mathbf{D}(s)}$$

where $\mathbf{N}(s)$ and $\mathbf{D}(s)$ are interval polynomials. Let

$$\underline{\mu}_{\mathbf{G}}(j\omega) := \inf_{G \in \mathbf{G}} |G(j\omega)| \quad \text{and} \quad \bar{\mu}_{\mathbf{G}}(j\omega) := \sup_{G \in \mathbf{G}} |G(j\omega)|$$

with similar definitions holding with $\mathbf{G}(s)$ replaced by $\mathbf{G}_E(s)$. Prove the following formulas for computing the extremal Bode magnitude values for interval systems:

$$\underline{\mu}_{\mathbf{G}}(j\omega) = \underline{\mu}_{\underline{\mathbf{G}}_{\mathrm{E}}}(j\omega) \qquad \bar{\mu}_{\mathbf{G}}(j\omega) = \bar{\mu}_{\bar{\mathbf{G}}_{\mathrm{E}}}(j\omega)$$

where

$$\underline{\mathbf{G}}_{\mathrm{E}}(s) := \frac{\mathcal{S}_N(j\omega)}{\mathcal{K}_D(j\omega)} \qquad \bar{\mathbf{G}}_{\mathrm{E}}(s) := \frac{\mathcal{K}_N(j\omega)}{\mathcal{S}_D(j\omega)}$$

8.3 In the interval system considered above in Exercise 8.2, prove the further simplification for computing extremal Bode angle values:

$$\underline{\phi}_{\mathbf{G}}(j\omega) = \underline{\phi}_{\mathbf{G}_{\mathrm{K}}}(j\omega) \qquad \bar{\phi}_{\mathbf{G}}(j\omega) = \bar{\phi}_{\mathbf{G}_{\mathrm{K}}}(j\omega)$$

8.4 Prove that

$$\frac{1}{\lambda d_0 + (1-\lambda)d_1}, \quad \lambda \in [0, 1]$$

where d_0 and d_1 are arbitrary complex numbers, is an arc of a circle. The circle passes through the points $\frac{1}{d_0}$, $\frac{1}{d_1}$ and 0, the origin in the complex plane.

8.5 In the control system given in Figure 8.39

$$C(s) = \frac{2s^2 + 4s + 3}{s^2 + 3s + 4} \quad \text{and} \quad G(s) = \frac{s^2 + a_1 s + a_0}{s(s^2 + b_1 s + b_0)}$$

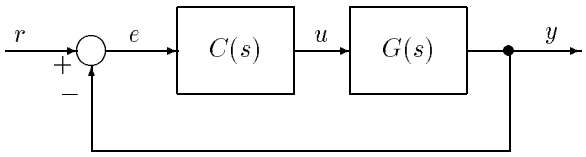

Figure 8.39. Feedback control system

with the nominal values of parameters being

$$a_1^0 = -2, \quad a_0^0 = 1, \quad b_0^0 = 2, \quad b_1^0 = 1.$$

Now let

$$a_0 \in [1-\epsilon, 1+\epsilon], \quad b_0 \in [2-\epsilon, 2+\epsilon]$$
$$a_1 \in [-2-\epsilon, -2+\epsilon], \quad b_1 \in [1-\epsilon, 1+\epsilon].$$

Assuming that $\epsilon = 0.0875$, determine

a) Bode envelopes of the open loop transfer function $C(s)G(s)$

b) From the Bode envelopes determine the worst case gain and phase margins of the system over the interval parameters

Answer: Gain margin=1.8014

c) Determine the worst case value over the parameter set, of M_p the peak value of the output transfer function evaluated over $j\omega$, for $\omega \in [0, \infty)$.

Answer: $M_p = 5.7075$

8.6 In the feedback system shown in Figure 8.39

$$a_1 \in (-2.115, -1.885), \qquad a_0 \in (6.885, 7.115)$$
$$b_1 \in (7.885, 8.115), \qquad b_0 \in (-0.365, -0.135)$$

Find the worst case gain and phase margin of the system.
Answer: $K^* = 5.6703$

8.7 Consider the block diagram given in Figure 8.39 with

$$a_1 \in [0.9, 1.1], \quad a_0 \in [-1.1, -0.9], \quad b_1 \in [-1.1, -0.9], \quad b_0 \in [1.9, 2.1].$$

Find the worst case gain and phase margins for the family by drawing the Bode magnitude and phase envelopes.

Answer: Gain margin=0.8358 = 1.55db. Phase margin=38.4381°)

8.8 In the control system shown in Figure 8.39

$$C(s) = \frac{20 + 30s + 12s^2}{-4 - 6s + s^2} \quad \text{and} \quad G(s) = \frac{a_0 + a_1 s + a_2 s^2}{s(b_0 + b_1 s + s^2)}$$

and the nominal plant transfer function

$$G^0(s) = \frac{1 + s + s^2}{s(1 + 2s + s^2)}.$$

Let

$$a_i \in [a_i^0 - \epsilon, a_i^0 + \epsilon], \qquad b_j \in [b_j^0 - \epsilon, b_j^0 + \epsilon], \qquad i, j = 0, 1, 2.$$

For $\epsilon = 0.2275$

a) Sketch the Bode magnitude and phase envelopes of the closed loop transfer function.

b) Find the worst case value of M_p.

c) Find the worst case gain and phase margins of the system.

8.9 For the system in Exercise 8.8, determine the worst case maximum steady state error over the parameter set when the reference input $r(t)$ is unit step.

8.10 Consider the stable interval transfer function $\mathbf{G}(s)$. Show that the steady state response with respect to step inputs for an interval transfer function is bounded by the steady state responses of its extremal systems $\mathbf{G}_{\mathrm{K}}(s)$.

8.11 NOTES AND REFERENCES

The boundary result of Theorem 8.2 is due to Tesi and Vicino [221]. The boundary result of Theorem 8.3 was reported by Keel and Bhattacharyya [132] and Keel, Shaw and Bhattacharyya [142]. The proofs of the frequency domain results of Theorems 8.4, 8.5, and 8.6 are given in Keel and Bhattacharyya [137]. In Bartlett [19] and Fu [98], the generation of frequency domain envelopes using the Edge Theorem is treated. The generation of Bode envelopes for interval plants are also dealt with by Bartlett, Tesi and Vicino [22]. Bartlett [20] showed that the extremal values of the steady state response of an interval plant for the case of multiaffine parameter dependencies are obtained from its vertex systems. Hollot and Tempo [117] showed that the Nyquist envelope of an interval family is *not* contained in the envelope of Nyquist plots of the Kharitonov plants. Applications of these frequency domain tools to classical control design, as described in Section 8.9, were reported in Keel and Bhattacharyya [135], Ahmad and Keel [5], and Ahmad, Keel and Bhattacharyya [6, 7].